Laura Ramos Serrano

Engenharia de Micro e Nanotecnologias

Bimetallic nanoparticles for highly sensitive colorimetric detection of glucose on paper

Dissertação para obtenção do Grau de Mestre em
Engenharia de Micro e Nanotecnologias

Orientador: Professora Doutora Elvira Maria Correia Fortunato, FCT-UNL

Júri:
Presidente: Prof. Doutor Rodrigo Ferrão de Paiva Martins
Arguente: Prof. Doutor Hugo Manuel Brito Águas
Vogal: Prof. Doutora Elvira Maria Correia Fortunato

FACULDADE DE CIÊNCIAS E TECNOLOGIA
UNIVERSIDADE NOVA DE LISBOA

Março 2020

Bimetallic nanoparticles for highly sensitive colorimetric detection of glucose on paper

"The power of imagination makes us infinite."

John Muir

Acknowledgements

Aproveito esta página para agradecer a todos aqueles que de alguma forma contribuíram para a conclusão desta etapa da minha vida.

Primeiramente, à Faculdade de Ciências e Tecnologia da Universidade Nova de Lisboa, por tão bem me ter acolhido, e em especial ao Departamento de Ciências dos Materiais pela qualidade de todo o pessoal docente e não-docente.

Um especial agradecimento à minha orientadora, Professora Elvira Fortunato, por todo o conhecimento transmitido, por toda a orientação dada e sobretudo por ter sido a grande impulsionadora do meu interesse por este curso.

À Carolina, por todo o apoio e preocupação que demonstrou ao longo do meu trabalho no CENIMAT. Obrigado por tudo!

A toda a equipa do CENIMAT, em especial à Sónia e à Alexandra pela disponibilidade e boa disposição. Ao Tomás, por todas as dicas. E à Daniela, pelo profissionalismo e gentileza que sempre demonstrou.

Aos amigos que fiz ao longo de todos estes anos e que sei que levarei comigo pela vida fora. Ao Branca, por todas as noites que passámos a rir e por tudo o que aprendi e aprendo contigo. Ao Xavier, Bernardo, Centeno, Narciso e Nuno: obrigado pela amizade, saídas, conversas e todos os momentos que vivemos juntos, tornaram estes anos muito especiais. À minha amiga Rijo, por todos os momentos bons, por toda a amizade e especialmente por me fazer sempre ver a vida com outra cor. À Lúcia e à Margarida, obrigado por toda a amizade, gargalhadas e conversas, vocês tornam bons até os piores momentos. Ao AD, por todo o apoio, amor e paciência. Obrigado pela paz e por teres feito de mim uma pessoa melhor.

Um obrigado muito especial à minha família, sem a qual teria sido impossível tornar-me a pessoa que sou. À minha irmã, pelo apoio incondicional, por ser a minha *partner in crime*, pelas viagens de carro a cantar clássicos, pelo tanto que me fez crescer: Obrigado! Uma tese inteira de obrigados não ia chegar. Aos meus avós, agradeço por tudo que fizeram por mim, por tudo o que aprendi com eles e por me fazerem sempre feliz. Finalmente gostaria de agradecer aos meus pais, que são a minha maior motivação e exemplo. Obrigado pela educação, pelo esforço, por todo o apoio e confiança que sempre depositaram em mim e, sobretudo, pelo amor. Sem vocês nada disto seria possível, obrigado!

Abstract

Diabetes Mellitus is a metabolic disease that affects 422 million people worldwide and is directly responsible for 1.6 M deaths per year, with an increasing incidence especially in low – and middle-income countries. It is characterized by high-blood glucose levels that may lead to severe damages on the patients' body tissues as blood vessels, eyes, heart, etc. The need to constantly monitor the blood glucose levels means a daily invasive blood collection that can be very stressful for the patient and frequently leads to a non-acceptance of the disease and the treatments. For this reason, glucose presence in other biofluids rather than blood is increasingly being studied, and it is possible to stablish a relation between the sweat glucose concentration values and the blood glucose levels in diabetic patients. Different enzymatic-based and electrochemical approaches have been taken for monitoring the low-glucose concentrations present in sweat, however most of these techniques are expensive and often relies on complex analysis of the results. For these reasons, in this work was developed a non-enzymatic paper-based colorimetric sensor for the detection of glucose in the range of hyperglycemic sweat glucose values (between 0.1 and 1 mM). The sensor is based on the glucose reduction of silver ions around disperse AuNPs adsorved on paper fibers, forming Au@Ag core-shell bimetallic NPs. The Ag-shell thickness increases with glucose concentration, resulting on colorimetric differences that may be quantified through digital analysis. Paper was utilized as substrate using the Lab-on-paper technology, where the deposition sites for glucose testing were defined by wax barriers diffused along the paper. Paper was chosen for being an abundant, biocompatible and low-cost material with good mechanical properties. Through RGB intensity measurement of the colorimetric results, a linear relation for glucose levels in a range from 0.12 to 1 mM was obtained.

Keywords: Paper biosensor; colorimetric assay; bimetallic nanoparticles; sweat glucose; enzyme-free.

Resumo

A Diabetes mellitus é uma doença que afecta 422 milhões de pessoas em todo o mundo, sendo responsável por 1.6 milhões de mortes por ano, com uma crescente incidência especialmente em países subdesenvolvidos. A doença manifesta-se através de elevados níveis de glucose no sangue, que poderão originar graves danos em diferentes tecidos do corpo, como veias, olhos, coração, etc. A necessidade de monitorizar constantemente o nível de glucose através de coletas de sangue, é origem frequente de stress e ansiedade, levando muitas vezes à não-aceitação da doença/tratamento por parte do individuo portador da doença. A detecção de glucose em bio-fluidos diferentes do sangue tem sido explorada, sendo possível estabelecer uma relação entre os níveis de glucose no sangue e no suor de pacientes hiperglicémicos. Existem diferentes abordagens desenvolvidas com vista a medir os baixos valores de glucose detectados no suor; no entanto, na sua maioria são técnicas dispendiosas e/ou dependentes de uma complexa análise de resultados. Por estas razões, neste trabalho foi desenvolvido um sensor colorimétrico não-enzimático em papel, para a detecção de glucose em concentrações similares às encontradas no suor humano (entre 0.1 e 1mM). O sensor baseia-se na formação de uma camada de iões prata, reduzidos pela glucose, em torno de nanopartículas de ouro adsorvidas nas fibras do papel, originando nanopartículas bimetálicas. A espessura da camada de prata aumenta com a concentração de glucose, produzindo diferenças colorimétricas visíveis, que podem ser quantificadas recorrendo a análise digital. O papel foi escolhido como substrato pela sua abundância, biocompatibilidade, baixo-custo e boas propriedades mecânicas, tendo sido utilizada a tecnologia Lab-on-paper para a definição dos poços de amostragem. Através da análise da intensidade da cor dos resultados obtidos em papel, foi possível definir uma relação linear entre estas intensidades e concentrações de glucose entre 0.12 e 1 mM.

Palavras-chave: Biosensor em papel; sensor colorimétrico; nanopartículas bimetálicas; glucose no suor; não-enzimático.

Abbreviations

a.u. – Arbitrary Units

AuNPs – Gold nanoparticles

AgNPs – Silver nanoparticles

CENIMAT – Centro de Investigação de Materiais

EDXS – Energy Dispersive X-ray Spectroscopy

FTIR – Fourier-Transform Infrared Spectroscopy

LOD – Limit of Detection

LOQ – Limit of Quantitation

NP - Nanoparticle

RGB – Red Green Blue

SEM – Scanning Electron Microscopy

SPR – Surface Plasmon Resonance

LSPR – Localized Surface Plasmon Resonance

UV-Vis – Visible and Ultraviolet radiation

XRD – X-ray Diffraction

µPADs – Microfluidic Paper-based Analysis Devices

Symbols

Au – Gold

Ag SIlver

C – Carbon

$CaCO_3$ – Calcium carbonate

$\boldsymbol{Cl}$ – Chloride

H – Hydrogen

Na – Sodium

O – Oxygen

OH – Hydroxide

g – Grams

mg – Milligrams

mL – Millilitres

µm – Micrometer

µL – Microliter

µg – Microgram

cm^2 – Centimeter squared

cm^{-1} – Centimeter high to minus 1

mM – Millimolar

M – Molar

keV – Kilo electron-volt

° - Angle

°C –Celsius degrees

% - Percentage

θ - Bragg Angle

$I_{(AM)}$ – Intensity for amorphous material

$I_{(200)}$ – Intensity for 200 peak

$\boldsymbol{m}$– Slope

$\boldsymbol{Sa}$– Standard deviation

CI – Crystallinity Index

Table of Contents

List of Figures

List of Tables

Motivation and objectives

According to the World Health Organization, Diabetes Mellitus is a chronic, metabolic disease that affects 422 million people worldwide and is one of the main causes of death in the world, especially in low- and middle-income countries. The disease is the responsible for 1.6 M deaths per year and is characterized by high blood glucose levels, that overtime may lead to the damage of several tissues of the human body as the blood vessels, eyes, kidneys, heart and nerves in general. For a diabetic patient who constantly needs to monitor the blood glucose levels, this means a daily invasive blood collection that causes stress and often leads to the non-acceptance of the disease and the treatments.

In this way, the development of painless and non-invasive glucose monitoring devices is an urgent need to improve the quality life of diabetes patients. To do so, other biofluids can be considered, such as sweat glucose, whose values are already proven to be related to the blood glucose levels. These glucose values, however, are present in sweat in very low concentrations (0.01 to 1 mM), making it very difficult to detect and quantify. Different approaches based on enzymatic or electro-chemical processes has been taken in the field of glucose detection in biofluids distinct than blood, however most of these techniques are expensive, time-consuming and unable to access for developing countries.

The challenge in this work is then to develop a non-enzymatic sensing platform for low-glucose values detection, utilizing the Lab-on-Paper technology to create a simple, rapid and low-cost paper colorimetric sensor. Hence, the principal steps taken towards the final objective of this work were:

i. Characterization of different paper types to be applied as substrate for the colorimetric sensing platform, developed using Lab-on-Paper technology;

ii. Study and development of a non-enzymatic protocol for the synthesis of Au@Ag core-shell bimetallic NPs with glucose, on paper;

iii. Optimization and calibration of the colorimetric results obtained through digital analysis, using aqueous glucose solutions with different concentrations.

Introduction

1.1. Diabetes mellitus

The World Health Organization classifies diabetes mellitus as a chronic disease associated to a low production of insulin by the pancreas, or when the body does an inefficient utilization of this hormone. As insulin is responsible for blood glucose regulation, diabetic patients often suffer a hyperglycaemic[1] state, leading to severe damages in different body structures specially in the nervous and cardiovascular systems. [1] In the year of 2016, diabetes was the cause of 1.6 million deaths and its prevalence is quickly increasing, especially in middle and low-income countries, [2] as presented in **Figure 1**.

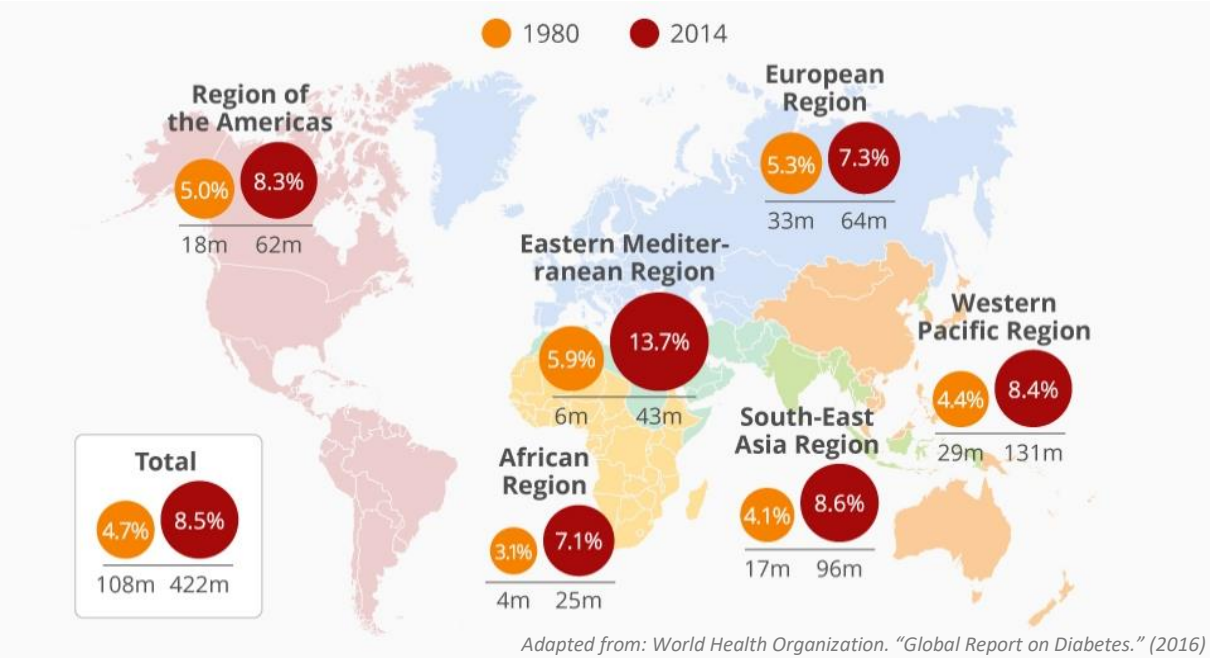

***Figure 1**- Percentage and number of adults with diabetes by WHO region in 1980 and 2014.*

Symptoms and complications associated to diabetes can be successfully minimized for diabetic patients who control their blood glucose levels daily, compensating eventual dysregulations by taking periodical insulin shots. [3] The pain and stress caused by these invasive regular blood collections along with resource-poor settings are the main reasons for patients not having their glucose levels monitored, that is why the search for inexpensive, non-invasive and painless methods for glucose measurement are highly desirable. [4], [5]

[1] Condition in which an excessive amount of glucose circulates in the blood plasma.

1.1.1. Sweat glucose as a biomarker

Sweat is typically a transparent biofluid with slightly acidic nature (pH between 4.5 and 7) that appears on the skin surface and is composed mostly of water (≈ 99%). [6] Produced by secretory glands that are distributed over the entire human body (eccrine sweat glands), sweat contains a wide range of health-related biomarkers including glucose, lactate, uric acid and electrolytes like Na^+ and K^+, making it a potential diagnostic biofluid. [7]

Since sweat glucose levels can accurately reflect the blood glucose concentration values [8], the investigation of sweat for diabetes monitoring has increasingly been developed. Sweat glucose can achieve concentrations of approximately 0.01 mM for hypoglycaemic patients and from about 0.1 to 1 mM in hyperglycaemic patients, [9] which is much lower than the glucose values in blood samples, increasing the difficulty of its detection in sweat using conventional techniques. As sweat is secreted on the skin surface, a non-invasive sample collection is possible using a simple sweat patch, which is a great advantage when comparing to the invasive commonly used blood sampling that further need to be processed for protein removal, increasing the difficulty and cost of the process; [10], [11] however, sweat testing remains a challenge as different skin areas reveal different quantities of sweat glands, influencing the volume and quantity of biomarkers expelled. Thus, sweat sampling is preferably done on the flexor surface of the forearm where the eccrine sweat glands are abundant and homogeneously distributed. [9], [12]

1.2. Biosensors

Biosensors are analytical devices defined by its biological receptor that recognizes and interacts with a specific analyte. [13], [14]Depending on the biological receptor, biosensors can detect and quantify from complex DNA sequences to simpler molecules such as glucose or water pollutants. [15] The interaction of the receptor with the analyte may generate different types of signals as electrochemical, electroluminescent, magnetic or optical, depending on the transduction[2] mechanism utilized. [16] Being responsible for the translation of the interaction analyte-receptor to a measurable signal, transducers may be more or less sensitive, depending on its detection limits.

Several factors impact the applicability of each sensor, as the fabrication techniques, the materials and sources utilized, or also the required data processing system, which often relies on time-consuming and expensive methods.[17], [18] For instance, enzyme-linked immunosorbent assay (ELISA) is a widely used immunological biomarker detection method to detect and quantify analytes in blood, urine, and serum; [19] although it provides sensitive, consistent, and very accurate results, due

[2] Process that converts a biochemical signal into another type of signal.

to long and complex procedures, the requirement of specialized personnel to both perform the assay and analyse the results, as well as the necessity of large volumes of reagent samples, makes it not the ideal analytical tool in resource-poor settings. [20], [21] Therefore, also in the field of medical diagnostics arises the necessity of developing fast, accurate, simple and low-cost devices.

1.2.1. Paper-based biosensors

Paper as a potential substrate for microfluidic biosensors has been explored to achieve the manufacture of simple, low-cost, portable, and flexible medical diagnostic platforms (paper-based biosensors).[22] Paper is an increasingly studied material since it has characteristics that make it interesting not only structurally but also chemically. It can be obtained from different and abundant sources such as wood, cotton, hemp, etc. and its properties may be selected depending on the paper intended application. [23] For biosensing applications, paper intrinsic characteristics as surface porosity, density, weight and thickness are extremely significant, because these features will influence the liquid mobility trough the paper devices. [24], [25] Cellulose fibres hydrophilicity nature promote the wicking of liquids along the paper volume and length [26], and so, for microfluidic applications it is desirable a paper type with enough porosity to allow a rapid fluid diffusion; furthermore, the thickness of the paper has a direct impact on the device performance, as if it is too thick higher sample volumes will be necessary. On other hand, if the paper substrate is excessively thin, the tensile strength will be affected making it more delicate and so more prone to damage during handling; [23], [27] for colorimetric detection specifically, paper thickness may be optimized for enhancement of the signal. [23]

There are different fabrication techniques for microfluidic paper-based biosensing devices (µPADs), such as photolithography,[28] inkjet printing, [29] stamping, [30] cutting, [31] screen-printing, [32] and wax printing. [33] Paper-based microfluidic technology consists, thus, of a simple approach that doesn't require an external energy to function. By the use of hydrophobic materials, microfluidic channels are patterned on paper, creating a path that will lead the sample to the detection zone by capillary forces, where the detection of the analyte occurs. Here, a chemical reaction will induce a change in the paper color, electrochemical properties, or light absorption/emission values. [34], [35]

Detection methods based on colorimetric variations may not simply indicate the analyte presence but can also provide quantitative information, meaning that it is possible to correlate the color change with the analyte concentration. [36] Depending on the sensor type, color change results can either be observed through naked-eye or also through software analysis of images taken by a scanner or even a mobile phone camera. Numerous paper-based colorimetric sensors have been developed to test different target analytes, such as glucose, protein biomarkers, and DNA sequences. [37]–[39]

1.3. Noble metal nanoparticles in biosensors

As mentioned before, several approaches have been taken to develop colorimetric biosensors, the majority of which relying on enzymatic processes. There is, however, a growing demand for non-enzymatic methods for biomarkers detection, as enzymes require specific pH and temperature conditions and are generally quite sensitive and cannot be stored for long periods. [40] Also, the cost of manufacturing non-enzymatic biosensors is lower as enzymes are relatively expensive compared to reagents used in non-enzymatic reactions. [41]

Metallic nanoparticles such as gold and silver nanoparticles (AuNPs and AgNPs, respectively) are increasingly being explored as colorimetric, chemical, and biological indicators, being widely used in biomarkers sensing for their unique optical properties. Noble metal nanoparticles show a very strong localized surface plasmon resonance (LSPR) (**Figure 2**), which can be traduced by the interaction of the electromagnetic field of incident light (UV-Vis) with free electrons on the NPs surface. [42] This interaction results in a collective oscillation of the conduction band electrons (plasmon resonance) with a certain frequency which strongly depends on the dimension, morphology and interparticle interactions of the NPs [43]-[45].

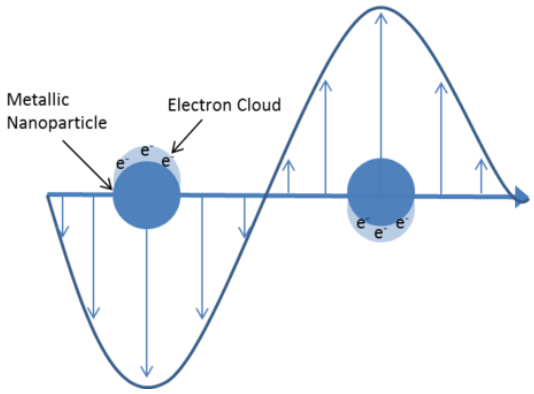

***Figure 2**- Localized surface plasmon resonance in metallic nanoparticles (LSPR). Adapted from[65]*

1.3.1. Gold nanoparticles (AuNPs)

AuNPs application in biosensing and recognition of various analytes has been increasingly explored in recent years. Their excellent biocompatibility, strong LSPR, conductivity, large surface to volume ratio and catalytic properties provide different applications for AuNPs in biosensors fabrication. [46] LSPR size and shape dependence in AuNPs are applied essentially in optical biosensing, as small NPs of around 10 nm in diameter absorb green light (absorption band at ≈ 520 nm), while in larger NPs the band absorption wavelength increases because light polarization of the nanoparticles ceases to be homogeneous. As a result, a solution containing small AuNPs appear red in colour,

changing to a purple/blue coloration if the particle size increase (this phenomenon is also observed during the aggregation of AuNPs, as it can be considered a single larger particle [47]). [48], [49]

The operation of a colorimetric sensor based on detection with AuNPs is supported by the relation between the NPs size increasing/aggregation induced by a specific analyte, with the solution colour changes.

1.3.2. Au@Ag core-shell bimetallic nanoparticles for glucose sensing

Different approaches have been developed to improve the use of metallic NPs in colorimetric sensing. One of the most evident and simplest strategies adopted to enhance the spectral response of AuNPs was by changing its morphology, like oval-shape or bimetallic nanoparticles. [50], [51]

One of the most effective methods for lowering the glucose concentration limit of detection on sensors are based on Au@Ag core-shell nanoparticles, where the rection product of glucose and glucose oxidase – hydrogen peroxide H_2O_2 – will etch the silver shell, causing a change in the solution colour. [52], [53] These techniques, however, rely on sensitive and very unstable enzymes, along with a complex and time-consuming preparation of the Au@Ag core-shell NPs. [54], [55]

These drawbacks lead to the development of a more controllable and stable system, based on a silver precursor - $[Ag(NH_3)_2^+]$ - called Tollens' reagent, that in the presence of glucose will do the inverse process instead and generate metallic Ag around the AuNPs. The reaction between glucose molecules and Tollens' reagent occurs in an aqueous solution containing dispersed AuNPs, in which surface Ag^0 is reduced, forming the Au@Ag core-shell nanoparticles which leads to a wavelength shift and consequentially to a change in the solution colour. [55], [56] (**Figure 3**)

$$2\,Ag(NH_3)_2OH + C_6H_{12}O_6 = 2\,Ag + C_6H_{12}O_7 + 4\,NH_3 + H_2O \quad (1)$$

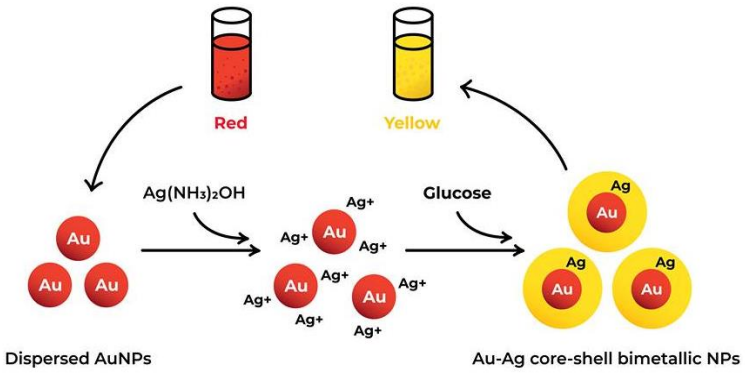

***Figure 3**- Schematic Au@Ag core-shell bimetallic NPs formation.*

A new approach combining this technique with a paper-based sensing platform is studied on the present work, with a view on the development of a simple, rapid and low-cost biosensing device for low glucose concentration levels.

Experimental Methods and Materials

2.1. Reagents preparation

2.1.1. Synthesis of gold nanoparticles by citrate reduction

The synthesis of AuNPs was made by citrate reduction (*Turkevich* method) which consisted in boiling 95 mL of an aqueous solution of hydrogen tetrachloroaurate (III) trihydrate ($HAuCl_4 \cdot 3H_2O$) in reflux setting until the temperature reaches 100°C; at this point, 5mL of a sodium citrate (1% w/v) solution was added under vigorous stirring and the reaction was allowed to proceed for 30 min and subsequently cooled to room temperature. The colloidal gold solution was stored at 4°C in the dark.

2.1.2. Diammine silver (I) hydroxide ($[Ag(NH_3)_2]OH$) preparation

Tollens' reagent ($[Ag(NH_3)_2]OH$) was prepared based on previous work [56]. 400 µl of $AgNO_3$ 0.1 M was mixed with 200 µl of NaOH 0.8 M, forming a brown precipitate. Then, 70 µl of ammonia [15 M] was added and slightly stirred until the brown precipitate dissolved. This solution should be prepared just before use to prevent precipitation.

2.2. Glucose concentration sensing

2.2.1. Glucose sensing in solution

To achieve a sensitive detection of glucose in solution and according to previous work [56], 2 ml e*ppendorf* tubes were placed in a *ELP Scientifica* vortex mixer; subsequentially, 20 µl of the colloidal solution of AuNPs (prepared in ***2.6.1.*),** plus 145 µl of distilled water and 15 µl of $[Ag(NH_3)_2]OH$ were added to each e*ppendorf*. After stirring for approximately 10 min, 20 µl of glucose with increasing concentrations from 0 to 1 mM were added to the *eppendorf* tubes and manually stirred for 30 sec. The reaction was allowed to proceed for 15 minutes (without stirring) at room temperature.

2.2.2. Glucose sensing on paper

With the aim of reproducing the reaction described in ***2.2.1.*** on paper, a variety of tests were performed on several paper microplates that were produced based on the Lab-on-Paper technology [57]. Using Adobe Illustrator, 96-well microplates were drawn (the wells are 7 mm in diameter and 1 mm distanced from each other). The drawn microplates were wax printed on A5 size sheets of Whatman paper nº1, using a *Xerox ColorQube 8570* printer. Lastly, the wax diffusion was made using a *SCHOTT ROBAX* hot plate at 120°C for about 3 minutes.

Different reagent concentrations and volumes were tested, as well as several reaction conditions, until the following optimal protocol was developed:

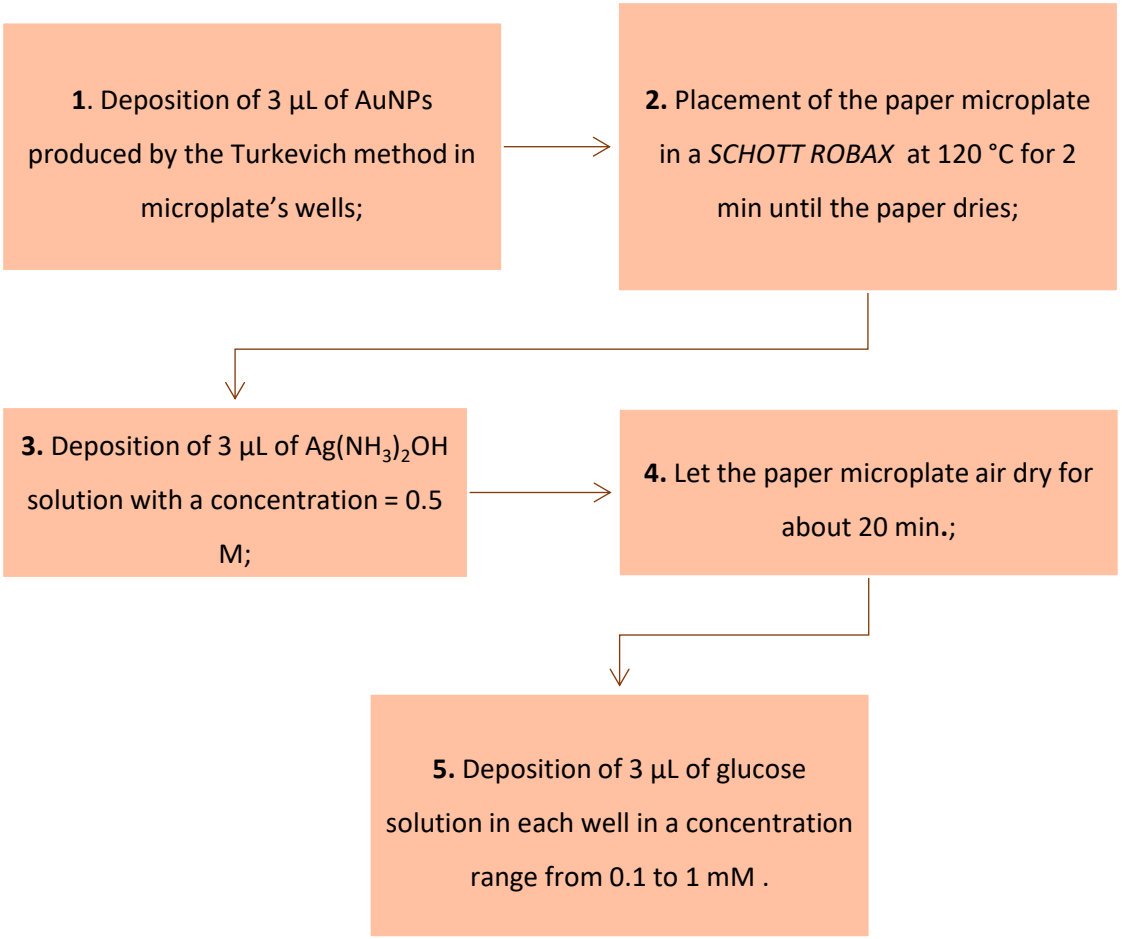

2.3. Characterization Techniques

2.3.1. NP's characterization on solution

Using a *TECAN SPARK 10M* microplater reader, the absorbance spectrum of the Au@Ag core-shell bimetallic NPs in response to different concentrations of glucose was analysed. To perform the UV-visible analysis, 200 µl of each solution with different glucose concentrations (prepared in 2.2.1) were deposited in a 96-well polystyrene microplate. SEM-EDS was used to characterize the bimetallic NPs in solution. To do so, 2 µl of solutions with different glucose concentrations were deposited on silicon and placed in a desiccator and left to dry overnight at room temperature.

2.3.2. Paper characterization

To choose the appropriate paper type for the development of a microfluidic paper-based device for colorimetric detection, different paper characterization tests were performed, such as: Fourier-Transform Infrared Spectroscopy (FTIR, *Nicolet 6700* from *Thermo Electron Corporation*), Scanning

Electron Microscopy (SEM, *Carl Zeiss AURIGA FIB-SEM Croossbeam*) coupled with Energy Dispersive X-ray Spectroscopy (EDS) and Xray Diffraction (XRD, *PANalytical X'Pert Pro*).

2.3.3. NP's characterization on paper

In order to observe and characterize the formation of the Au@Ag core-shell bimetallic nanoparticles on paper, SEM and EDS techniques were used at different stages of the process.

2.3.4. Digital Analysis

To quantify the color alterations, the paper microplates were scanned with a *Cannon MG5250* scanner and later the RGB mean intensities of the wells were analysed using *ImageJ* software.

Results and Discussion

The results obtained in this work are presented and discussed in this chapter. Firstly, the paper substrate selection is made, supported by structural, morphological and chemical characterization. Then, the glucose detection capability of the proposed strategy is evaluated in solution, followed by different strategies for the optimization of the reaction on paper. Finally, validity tests on paper were performed for different types of environments.

3.1. Paper Characterization

Different types of paper were studied in order to select the most suitable substrate to develop a paper-based microfluidic device for colorimetric detection. The selection was made between Whatman chromatography paper grade 1 and common office paper; a chemical, morphological and structural analysis of both types of paper were performed.

3.1.1. FTIR

A chemical analysis of both paper types was done using Fourier-Transform Infrared Spectroscopy (FTIR) to identify the chemical bonds and functional groups present in each type of paper. The FTIR spectra obtained and respective peak identification are present in **Figure 4**.

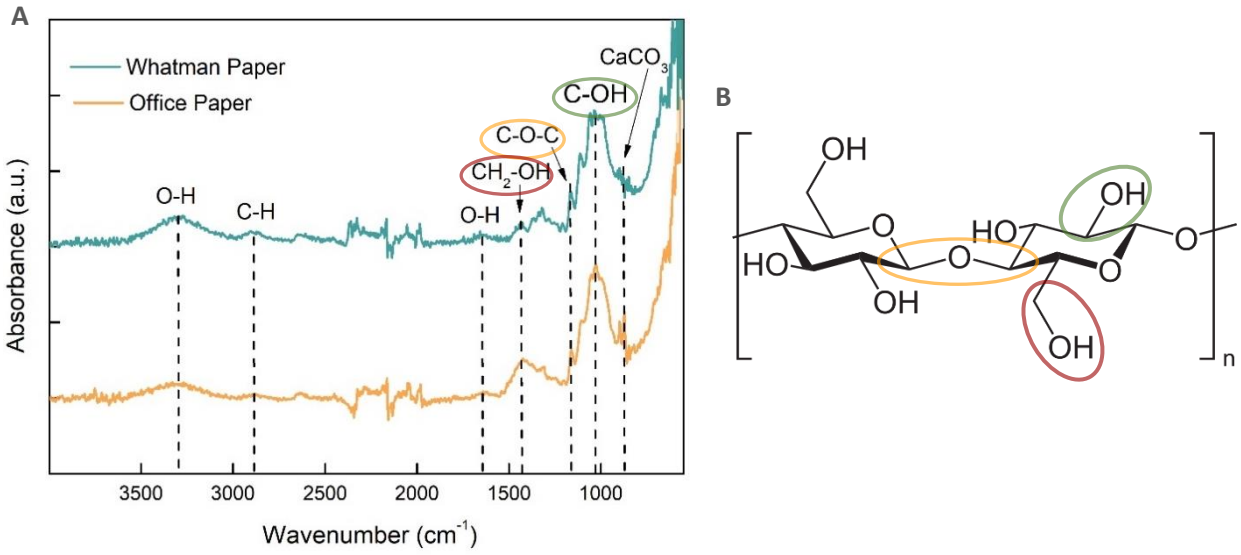

***Figure 4**- FTIR spectra of Whatman and office paper (A) and cellulose chemical structure (B) with the identification of the chemical bonds corresponding to the characteristic peaks of cellulose.*

Analysing the FTIR spectra present in **Figure 4** is possible to observe two peaks, at wavenumbers 3303 and 2885 cm^{-1}, characteristic of O-H and C-H bond vibrations in polysaccharides. In the range of 1500 to 900 cm^{-1}, several coincident peaks can be detected in both infrared spectra, corresponding to the characteristic peaks present in the structure of cellulose (**Figure 4-B**). In this spectra area named fingerprint region, is possible to identify at 1424, 1163 and 1023 cm^{-1} the peaks corresponding to stretching and bending vibrations of CH_2-OH (red), C-O-C (yellow) and C-OH (green) bonds,

respectively. At wavenumber 1641 cm^{-1}, a peak associated to the vibration of water molecules absorbed in cellulose can be distinguished. [58]

Comparing both papers spectra, it can be observed the absence of a peak at 873 cm^{-1} in Whatman paper that is present in office paper. This peak corresponds to C-O vibrations associated to Calcium Carbonate ($CaCO_3$), revealing the presence of this compound in office paper. [59]

3.1.2. SEM

The differences in surface morphology between the two types of paper substrates were analysed trough Scanning Electron Microscopy (SEM). Is possible to observe in **Figure 5** SEM images of Whatman paper and Office paper.

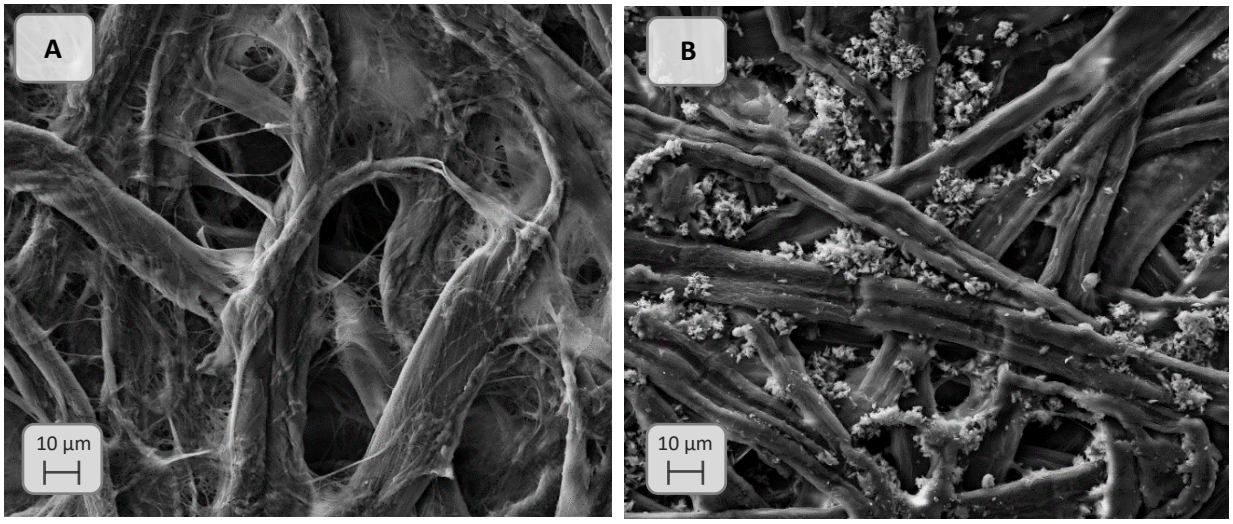

***Figure 5**- SEM images of the studied papers. (A) Whatman paper (B) Office paper.*

Through observation of the previous SEM images is possible to confirm that both paper substrates are composed of cellulose fibres arranged on a three-dimensional network. However, this arrangement of cellulose fibres has differences from one type of paper to the other, since Whatman paper presents higher porosity and larger pores, while office paper shows a higher density of fibres, being evident the presence of crystalline agglomerates filling the majority of the pores. These agglomerates may correspond to $CaCO_3$ (previously detected in FTIR analysis), since it is a bright white mineral added during paper manufacture to increase its brightness, opacity, and whiteness.

Regarding the fiber geometry, some distinctions are also notable, as Whatman paper fibres appear to be more cylindrical, whereas office paper fibres present a more flattened geometry. These dissimilarities directly impact the diffusion process and volume of fluids supported by the office paper substrate, as its thickness is lower when compared to Whatman paper.

3.1.3. EDS

Energy Dispersive X-ray Spectroscopy was used to confirm the presence of $CaCO_3$ inside the pores on office paper, since it provides information on relative abundances of the elements present in the sample. In **Figure 6** is presented the cumulative EDS spectra corresponding to an office paper SEM image.

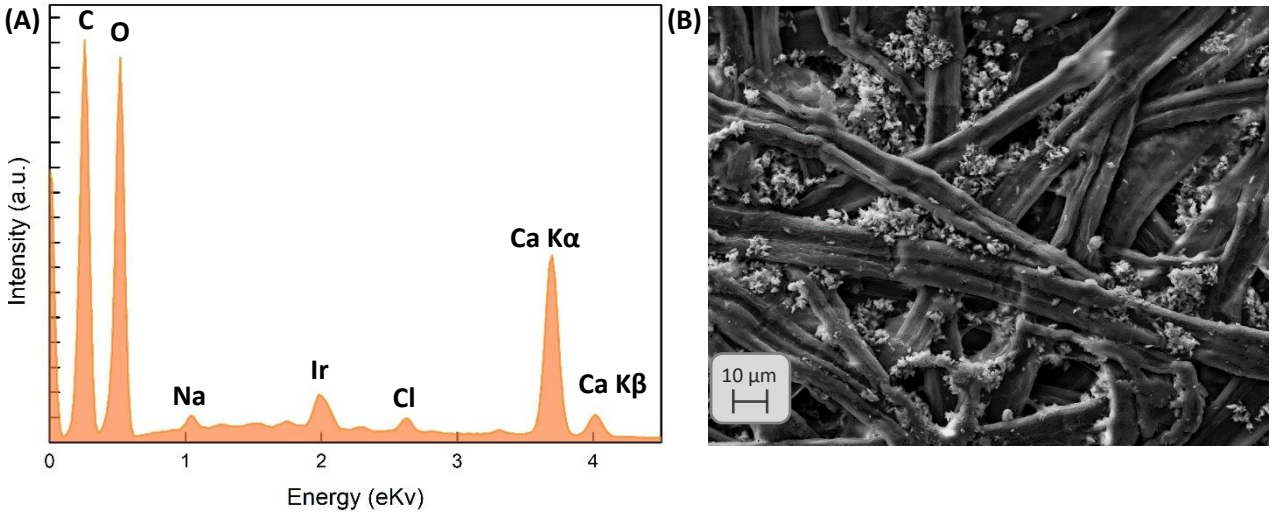

***Figure 6**- EDS analysis of office paper: (A) Cumulative spectrum of EDS analysis and (B) SEM image of office paper.*

The results obtained through EDXS analysis revealed that the sample is composed mainly by carbon and oxygen (E = 0.26 keV and E = 0.52 keV, respectively). It is also notable two peaks of considerable intensity associated to calcium (E = 3.7 keV and E = 4.0 keV). Three other elements were detected in lower amounts: sodium (E = 1.04 keV), iridium (E = 1.997 keV) and chlorine (E = 2.62 keV).

Since carbon and oxygen are the main components of cellulose[3], the high intensity peaks obtained for these two elements were expected. The detection of calcium peaks confirms the presence of $CaCO_3$, previously seen in SEM imagens and detected by FTIR. The presence of sodium and chlorine elements is justified because these are part of reactants utilized in paper industry: sodium hydroxide is used in the treatment of the cellulose fibres and chlorine for bleaching and give paper a whiter coloration. The peak associated to Iridium element is related to the coating layer used in this technique.

Along with information on relative abundance, EDS technique also provides information about the element distribution on the samples. The distribution maps of the three main components of office paper is presented in **Figure 7**.

[3] Note: hydrogen is also a main component of cellulose however this technique doesn't detect this element.

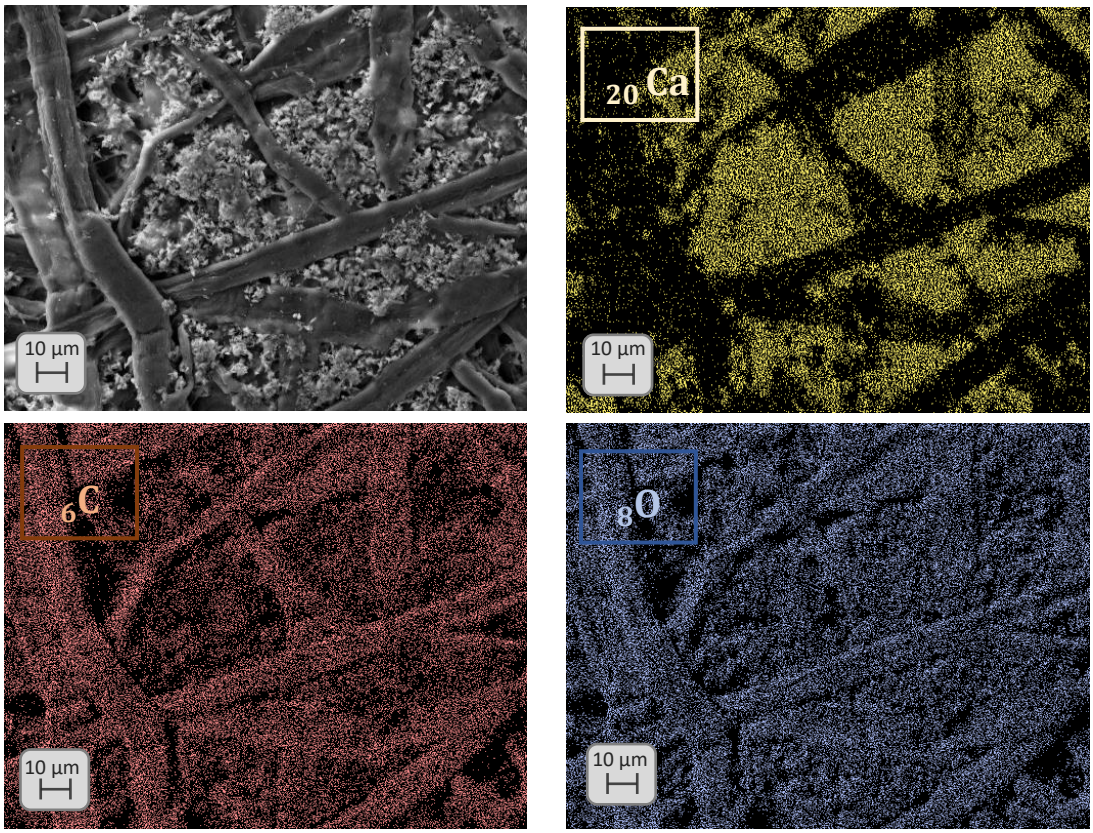

***Figure 7**- EDS distribution map of elements on office paper.*

Through visual inspection of the element distribution maps obtained for office paper, is possible to confirm that carbon and oxygen are present throughout the sample. Also, distribution map of calcium indicates that this element is present in smaller and specific areas, particularly between the cellulose fibres. Thus, is possible to associate the white agglomerates observed in SEM images to $CaCO_3$.

3.1.4. X-Ray diffraction

A structural analysis of both paper types was performed using X-Ray diffraction. In **Figure 8** are presented the obtained diffractograms for Whatman Paper and office paper, as well as the identification of characteristic peaks correspondent to the crystalline structures found on the samples.

Analysing the diffractograms is possible to identify the characteristic peaks of cellulose type I for both of paper types; however, while office paper presents one peak at 15.93°, in Whatman paper is possible to observe two separate peaks (at 14.96° and 16.50°), which are associated to two different crystalline structures existing in cellulose type I. This difference in the diffractograms is due to the fact that office paper has a greater amount of amorphous materials, such as lignin and hemicellulose, resulting in a singular and wide peak. Another characteristic peak for cellulose was detected in both paper types at 22.91°.

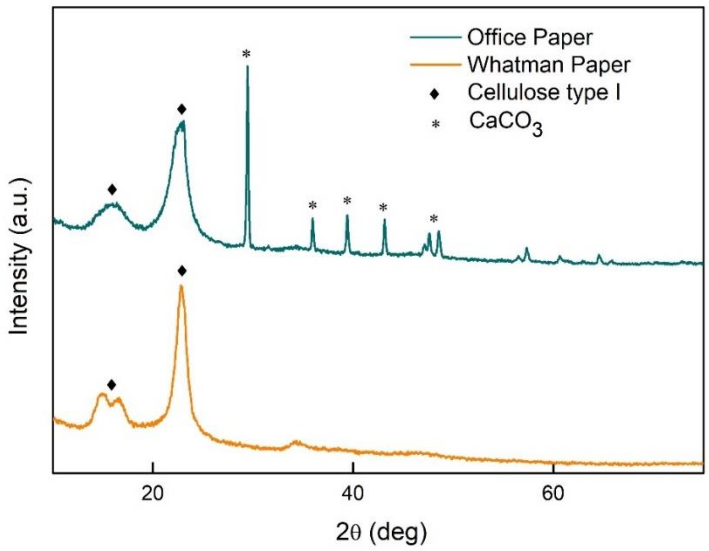

***Figure 8**- XRD diffractograms of Whatman and office paper and crystalline structurespeak identification.*

As expected from previous analysis, it is also possible to detect in the office paper diffractogram, different peaks associated to the crystalline structure of $CaCO_3$, confirming the presence of this compound on office paper.

The crystallinity index (CI) refers to the relative amount of crystalline material present in the studied samples and was determined using Segal's method [59], [60]:

$$CI(\%) = \frac{I_{(002)} - I_{(AM)}}{I_{(002)}} \times 100 \qquad (2)$$

That relates the peak intensity of the (002) plane for cellulose type I ($I_{(002)}$) with the intensity of the amorphous components of the sample ($I_{(AM)}$), that are given in the diffractograms by the minimum intensity peak between the (002) and (101) plans (at approximately 18.09° in **Figure 8**). It was calculated for both paper types and showed that Whatman Paper has a greater CI (74.71%) than office paper (67.48%), confirming the presence of a larger amount of amorphous material on office paper.

3.2. Sensitive glucose measurement in solution

Prior to any experiments on paper, the capability of the proposed strategy for low glucose concentration sensing was tested in solution, as described in section **2.2.1**.

The process used to form the bimetallic nanostructures is based on the reduction of silver ions present on Tollens' reagent ($[Ag(NH_3)_2]$) by glucose, on a medium with disperse and stable gold nanoparticles. The reaction will generate Ag^0 around the AuNPs that had been previously added to the system, forming the Au@Ag core-shell NPs. [56]

Solutions with different glucose concentrations were tested, to identify the relation between the optical properties of the obtained Au@Ag core-shell NPs and the glucose concentration level of the samples. In this work, as the sweat values for glucose concentration in diabetic and non-diabetic patients go from 0.11 to 1 mM, the concentrations of glucose chosen for test went from 0.1 to 1 mM (**Figure 9**).

***Figure 9**- Colour differences of Au@Ag core-shell bimetallic NPs colloidal solutions obtained with different glucose concentrations in a range from 0 -to -1 mM (left to right).*

Is possible to observe in **Figure 9** the gradual change in solution colours, from transparent to brown, indicating a variation in the size of the nanoparticles with the addiction of glucose.

3.2.1. UV-Vis Spectrophotometry

An UV-visible spectrophotometry measurement of the distinct coloured samples was performed in order to determine the relation between glucose concentration and the solution absorbance. The obtained absorbance spectra, in a range from 300 to 800 nm, is presented in **Figure 10**.

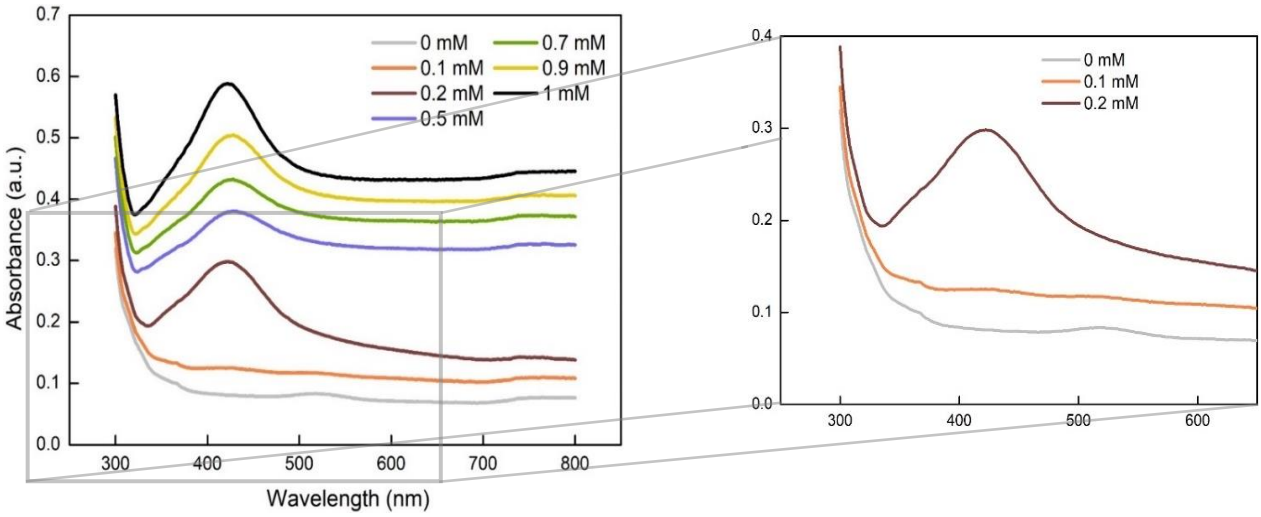

***Figure 10**- UV-Vis Absorbance spectra of solutions containing Au@Ag core-shell NPs obtained for different glucose concentrations.*

When no glucose is added to the system, it is possible to observe only one peak corresponding to the surface plasmon resonance of the AuNP present on the solution (**Appendices-A**). AuNPs synthetized through *Turkevich* method exhibit an SPR peak at a wavelength ≈ 520 nm that can be associated to an AuNP diameter size of approximately 10nm. [61]

The appearance of a peak at 422 nm in the UV-visible spectra presented on **Figure 10**, suggests the Ag^0 shell around AuNPs is starting to form, as the SPR peak for AgNPs of approximately 40 nm of diameter is between 420 and 423 nm. [62] It is possible to observe by analysing the graphic, at a wavelength of 422 nm, an increase in the maximum absorbance when increasing the glucose concentration, suggesting the formation of more Au-Ag bimetallic NPs, consequentially changing the colour solution.

From the detection of two absorbance peaks at 520 and 422 nm, when glucose concentration in the system is equal to 0.1 mM, it can be deduced that the Ag^0 shell around the AuNPs starts to occur near this concentration value (**Appendices-A**). Moreover, it is only possible to observe the occurrence of a very distinguishable SPR peak for glucose concentrations equal or above 0.2mM.

A calibration curve for glucose measurement was obtained for glucose concentrations from 0 to 1 mM, at the wavelength of 422 nm (**Figure 11**). Three measurements were made for each glucose concentration, whose standard deviation values are represented in the error bars.

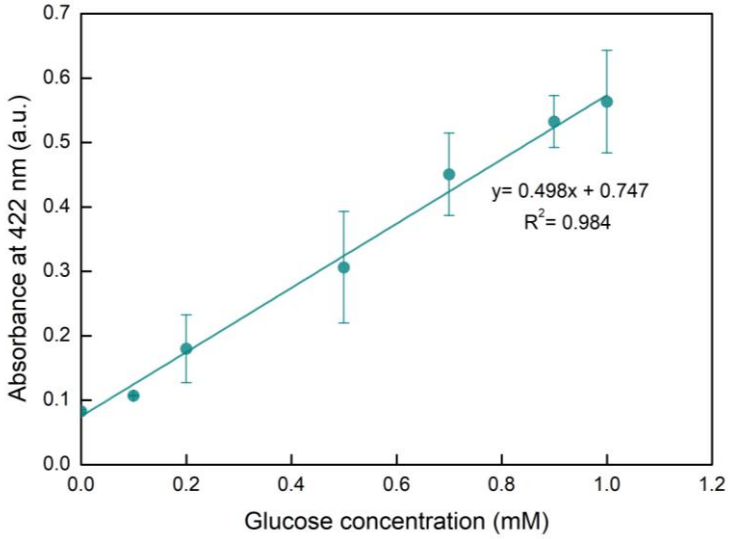

***Figure 11**- Calibration line obtained for the SPR peak absorbance variation (at wavelength = 422 nm) with glucose.*

The trendline obtained in **Figure 11** relates the SPR peak variation with each glucose concentration value, stablishing a linear relation, at 422 nm, between the absorbance and the glucose concentration in solution. This method for a sensitive glucose measurement in solution has a limit of detection (LOD) near 0.1 mM, as this was the lowest glucose concentration tested, and so it includes the range of sweat glucose values for hyperglycaemic patients.

3.2.1. SEM-EDS

A SEM-EDS analysis of the solutions was performed to observe the morphology of the Au@Ag core-shell NPs and its changes in the presence of glucose. The bimetallic NPs structure in solution was studied for glucose concentrations of 0.2 mM and 1 mM (**Figure 12**).

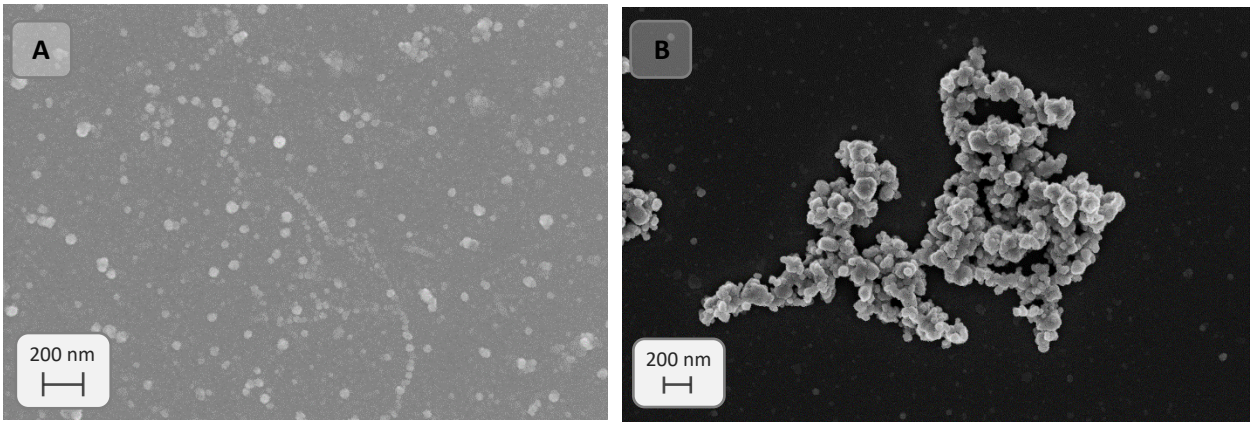

***Figure 12**- SEM images of bimetallic Au@Ag core-shell NPs obtained in solution with different glucose concentrations. (A) Glucose concentration of 0.2 mM. (B) Glucose concentration of 1 mM.*

SEM images corresponding to bimetallic NPs produced with 0.2 mM of glucose - **Figure 12- A**, presented a homogeneous distribution of small white dots corresponding to the Au@Ag core-shell NPs as will be discussed below on this section. Analysing the bimetallic NPs formed with a glucose concentration of 1 mM - **Figure 12- B**, it is possible to observe that they are in small aggregates distributed along the sample and presented a semi-spherical shape of bigger diameter in comparison with the previously observed NPs.

The EDS cumulative spectra of the samples containing 0.2 and 1 mM of glucose are presented in **Figure 13**.

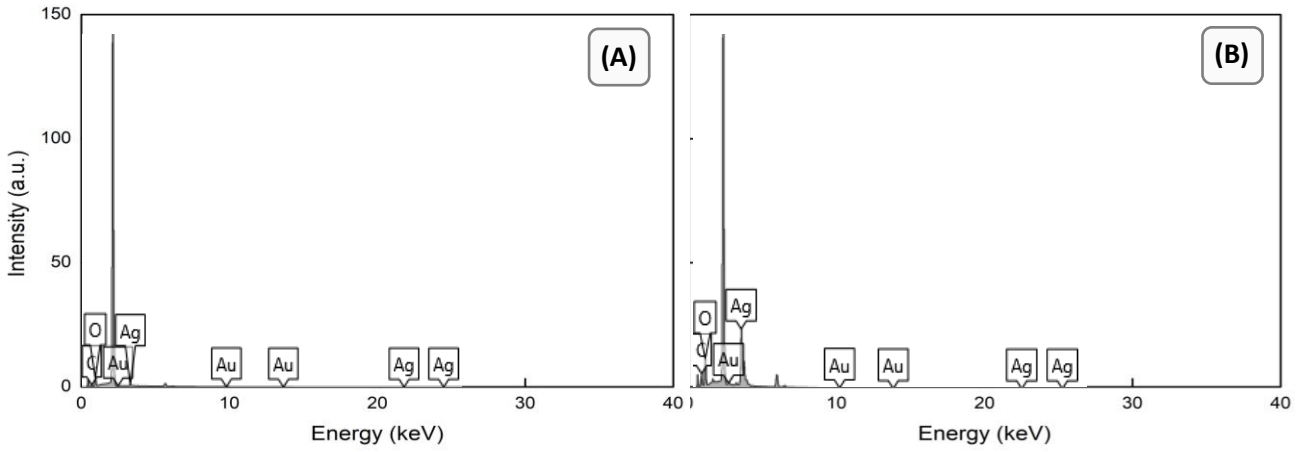

***Figure 13**- Eds cumulative spectra of Au@Ag core-shell NPs obtained with: (A) 0.2 mM of glucose and (B) 1 mM of glucose.*

Analysisng both spectra, is possible to detect the characteristic peaks associated to carbon (0.277 keV), oxygen (0.525 keV), gold (2.123, 9.713 and 11.443 keV) and silver (2.983, 22.163 and 24.941 keV). Even though the most energetic peaks associated to Au and Ag have almost negligible intensities in both spectra, a significant increase can be detected in the Ag peak intensity (at 2.983 keV) when rising the glucose concentration in the system.

In **Table 1** is summarized the average diameter of the observed bimetallic NPs as well as the ratio of the relative concentration of Ag/Au elements, measured by EDS analysis, in the 0.1- and 1-mM glucose samples(**Appendices- B**).

***Table 1**- Average diameter of the bimetallic NPs and relative concentration of Au/Ag elements for 0.1 and 1 mM of glucose*

Glucose concentration (mM)	Average Diameter (nm)	Relative concentration of Ag/Au (%)
0.2	39.738	3.607
1	115.707	31.308

The average diameter measured for the bimetallic NPs shows an overall increase (from ≈ 40 nm to 115 nm) when increasing glucose concentrations from 0.2 to 1mM. As expected from UV-Vis spectra analysis, the bimetallic is approximately 40nm

The relative concentration of Ag and Au elements in the observed samples reinforces the idea of having more formation of Ag^0 shell around the AuNPs when increasing the solution glucose concentration. Although EDS semi-quantitative analysis of chemical elements accuracy is strongly dependent on the nature of the sample, it can be noticed that the ratio between Ag and Au increases from around 3.6 to 31.30% when increasing glucose concentration.

3.3. Sensitive glucose measurement on paper

A sensitive detection of glucose in paper substrate was developed based on the formation of Au@Ag core-shell NPs using Tollens' reagent. Several approaches were tested, as well as different experimental conditions, in order to verify which path exhibited better results for the bimetallic NPs synthesis on paper.

Using office paper microplates as substrate, it was possible to observe some hydrophobicity of the material, hindering the sample adsorption onto the paper surface. This results in longer procedure times than the ones made with Whatman Paper nr1, and a much lesser uniform dispersion of the sample through the paper microplate wells. The observed experimental features, associated to the information acquired in section **3.1**, led to the use of Whatman paper as substrate for the sensitive glucose detection.

Different approaches were taken to synthetize the Au@Ag core-shell bimetallic NPs on paper, starting with varying the reactants deposition method. Initially, with a view to eliminate one deposition step, the colloidal solution of AuNPs produced by the *Turkevich* method was previously mixed with $Ag(NH_3)_2OH$ solution in a proportion of 1:1. After stirring, in each well of the Whatman paper microplate, 2.5 and 5 µl of this pre-mixed solution were deposited, in order to also see the deposition

volume influence on the reaction on paper; glucose was then added in different concentrations and the paper was left to dry in open air (**Figure 14**).

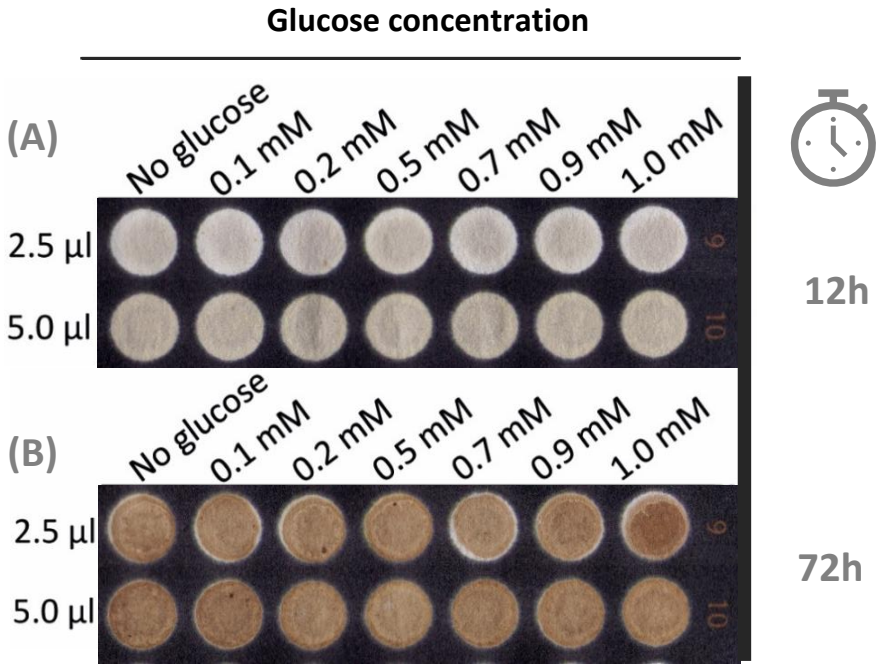

***Figure 14**- Whatman paper microplates containing 2.5 and 5 µl of the pre-mixed solutions of the Au-core and Ag-shell precursors with different glucose concentrations. Scans were taken after: (A) 12h and (B) 72h of the deposition.*

Analysing **Figure 14** through naked eye, it is not possible to observe a significant colour variation on paper wells immediately or passed 12 hours of the glucose deposition; the paper presented a dark-brown coloration only after 72h have passed (**Figure 14-B**), that is believed to be silver sulfide (Ag_2S), a black compound product of the reaction of silver with the sulfur compound in the air. [63] No considerable differences between the wells with distinct glucose concentration can be detected, showing the ineffectiveness of this approach, as the objective is to be capable of distinguish the different glucose concentration by colour.

Also, the differences observed between the volumes deposited presented no variation on the colour intensities, but the appearance of a white ring around the deposition wells suggests that a volume of 2.5 µl may be insufficient to fill in the totality of the deposition sites.

Another deposition process was tested, which consisted of depositing separately on the paper wells the gold NPs in solution and the silver precursor. It was deposited 3 µL of the AuNPs colloidal solution and then the paper microplate was dried for 5 minutes on a heating plate. The same volume of $Ag(NH_3)_2OH$ solution was then deposited and air dried, followed by glucose deposition in a range of concentrations from 0 to 1 mM (**Figure 15**).

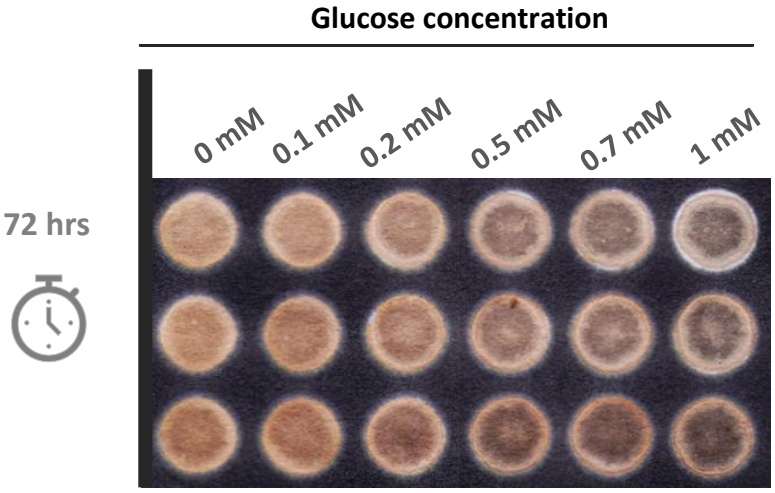

***Figure 15**- Paper microplate after 72 hours of the deposition in separated of the Au-core and Ag-shell precursors with increasing glucose concentration deposition.*

A few minutes before the silver-shell precursor ($Ag(NH_3)_2OH$) deposition, all the paper wells presented a light-yellow coloration but passed 72 hours it was possible to identify colour variation in all paper wells, revealing an intensification from light-brown to dark-grey as the glucose concentration increases. Observing **Figure 15**, the colour variation approximately corresponds to the previous observed colour changes in the bimetallic NPs synthesis in solution, indicating that larger particles or particle agglomerates are produced for higher glucose concentration on paper. However, the paper wells presented a non-homogeneous distribution of the sample, showing several less-colored spots on the center of the paper wells and also a white ring around the well limits, what may indicate an insufficient deposition volume. These details difficult the sample colour analysis and will lower the accuracy of the measurements.

A digital analysis of the obtained results was performed using *ImageJ*. With this software, the colour intensity of the samples was determined using the average RGB (Red + Green + Blue) channel values of each paper microplate well, and so a relation can be made between the well colour and the glucose concentration (**Figure 16**).

As expected from visual inspection, RGB analysis revealed significant colour intensity variation between the wells, being possible to distinguish in terms of intensity some of the studied glucose concentrations (**Figure 16 - a**). The RGB intensities for each channel are in a range from 0 to 255, being 0 correspondent to black and 255 to the white colour. [64] The observed decrease in the intensity mean of the RGB channels as glucose concentration increases, means that the sample colours are approximating to black. There are however some limitations observed, as for 0 and 0.1 mM of glucose where the mean colour intensities have very similar values (**Figure 16 - b**) and so the glucose range values between 0 and 0.1 cannot be accurately distinguished. Also, a great dispersion of results can be noticed, decreasing the assay accuracy.

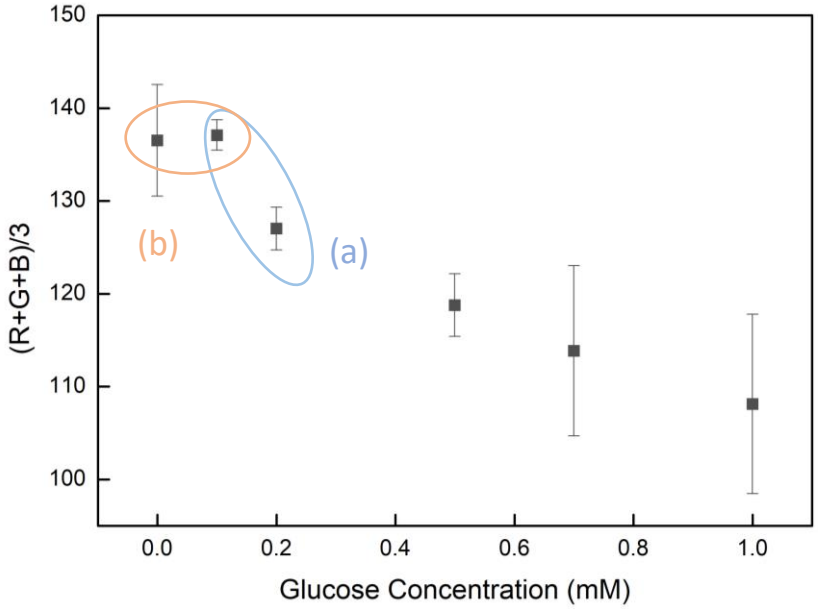

Figure 16- RGB channel mean intensities variation with different glucose concentrations on paper microplates containing the bimetallic NPs precursors deposited separately.

In order to overcome this limitations, the reactants' concentration influence on the Au@Ag core-shell NPs synthesis on paper was tested. Colloidal AuNPs with different concentrations were tested on paper, with results showing an enhancement of the signal for higher AuNPs concentration (**Appendices- C**). The reactants volume was also adjusted and 3.5 µL of each reactant was deposited in each one of the 96-well paper microplate.

The concentration of the silver-shell precursor ($Ag(NH_3)_2OH$) was then studied in a range from 0.1 to 1 M. Both of the bimetallic NPs precursors were dried on a hot plate at 80°C for 2 minutes after depositions, in order to accelerate the process (**Figure 17**).

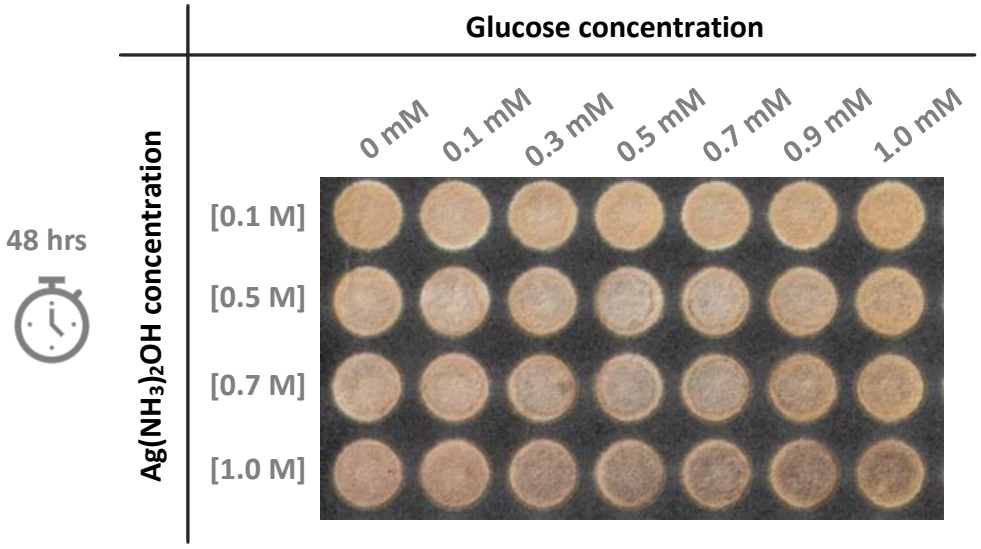

***Figure 17**- Influence of the silver-shell precursor [$Ag(NH_3)_2OH$] concentration on the Au@Ag core-shell bimetallic NPs synthesis on paper with glucose.*

After 48 hours is possible to observe that for a Tollens' reagent concentration of 0.1 M the wells presented no visible colour changes, suggesting that there are not sufficient Ag^+ ions to react with glucose, thus the shell around AuNPs was not formed.

The intensity of the grey colour on the wells (**Figure 17**) improves as increasing the silver shell precursor concentration, however, as observed from the previous experiments, the paper wells with a concentration of 1 M of the silver precursor showed stained and less homogeneous colourations that may be due to non-reacted silver aggregation.

In **Figure 18** are presented the RGB mean intensity values (**A**) and the calibration lines (**B**) for different concentrations of $Ag(NH_3)_2OH$, both relating the glucose concentration with the average of the three channels. The RGB analysis for all the four concentrations are presented in **Appendices- D.**

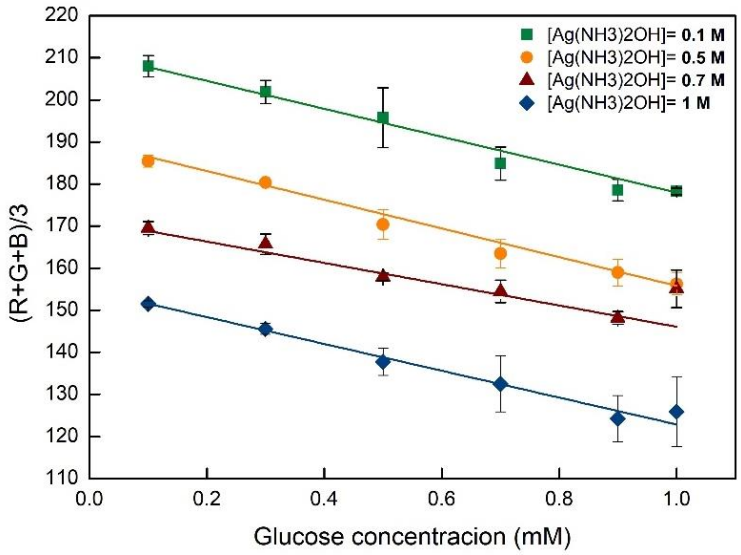

***Figure 18**- Calibration lines of the RGB analysis of the paper microplates containing different $Ag(NH_3)_2OH$ concentration.*

Analysing **Figure 18,** a significant difference between intensities of the four $Ag(NH_3)_2OH$ concentrations is observed. The decrease on the RGB channels intensity when rising $Ag(NH_3)_2OH$ concentration, means an approximation of the black colour (intensity value = 0), in agreement with the observed in the paper microplate wells in **Figure 17**.

It is possible to determine a linear relation for glucose concentrations between 0.1 and 1 mM for all the concentration tested, however, for $Ag(NH_3)_2OH$ at higher concentration, a large dispersion of results was observed (**Figure 18**). This may be related to the non-homogeneity of the sample distribution previously noticed on the paper microplates.

For a concentration of 0.5 M of the silver-shell precursor, the paper colorimetric analysis presented a greater uniformity of results, as well as a more accentuated distance between the 0 and 0.1 glucose concentration values when comparing to the other concentration values**.**

The linear calibration of the results is defined by

$$y = mx + b\ , \tag{3}$$

where RGB channel intensities (y) are related with the tested glucose quantities (x).

The sensitivity and the LOD were calculated for the four calibration lines and are presented in **Table 2**.

***Table 2**- Sensitivity and LOD of the calibration lines for the different $Ag(NH_3)_2OH$ concentrations.*

$[Ag(NH_3)_2OH]$	**0.1 M**	**0.5 M**	**0.7 M**	**1 M**
Sensitivity	33.173	34.089	25.299	31.874
LOD (mM)	0.228	0.125	0.185	0.159

The sensitivity is given by m (the slope of each calibration curve) and the LOD was calculated based on the expression

$$LOD = \frac{3Sa}{m}, \tag{4}$$

where Sa represents the standard deviation of the response.

Based on the observed differences and the obtained parameters in **Table 2**, 0.5 M was the chosen concentration for $Ag(NH_3)_2OH$ reactant, as it presented a lower LOD, meaning it can detect lower concentrations of glucose, presenting also a greater sensitivity.

However, as is noticeable on the paper microplate wells in **Figure 17** and by the higher RGB channel intensities initially measured, it can be assumed that the heat from the hot plate had influence on the colorimetric results, smoothing the colour differences. Consequentially, the heating step after the Ag-shell precursor deposition was eliminated and, under the optimized conditions, the colour variation was tested.

The paper microplates colorimetric variation showed a good linearity and reproducibility of results with glucose variation under the defined conditions; however, it is only possible to obtain measurable colour differences between the microplate paper wells after 48 hours (**Figure 19**).

In **Figure 19** is possible to observe a gradual colour change from light to dark brown along the paper wells, meaning that glucose concentration has a direct effect on the colouration presented on the samples.

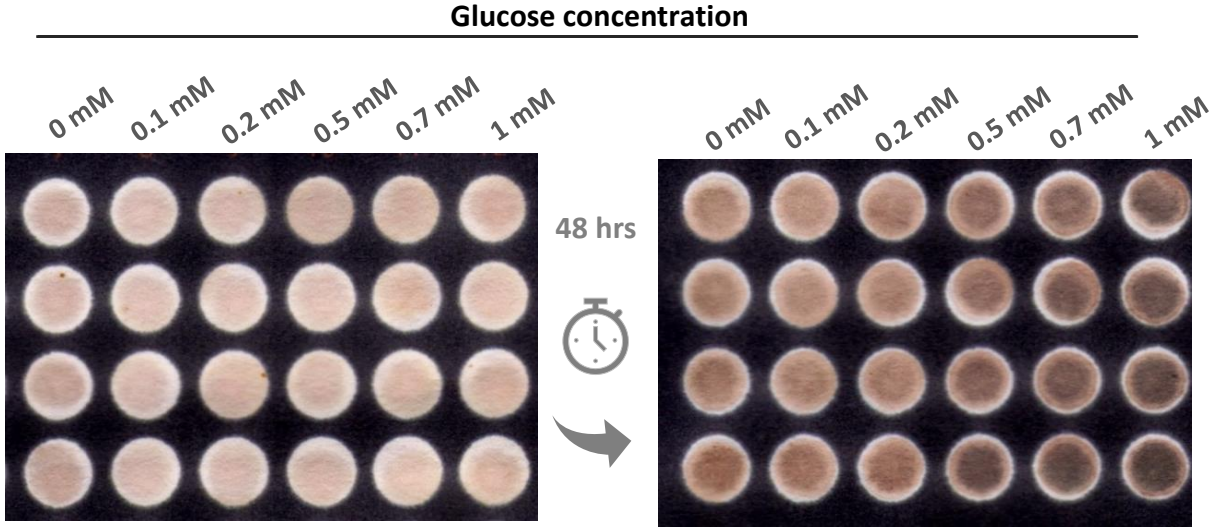

***Figure 19**- Au@Ag core-shell NPs formation on paper with glucose (after 48hrs) under the optimized precursor deposition conditions: 3.5 µl of AuNPs, followed by 3.5 µl of 0.5 M $Ag(NH_3)_2OH$ air dried.*

A calibration line was plotted to stablish a relation between the RGB channel mean intensities and the glucose levels for the optimized conditions (**Figure 20**).

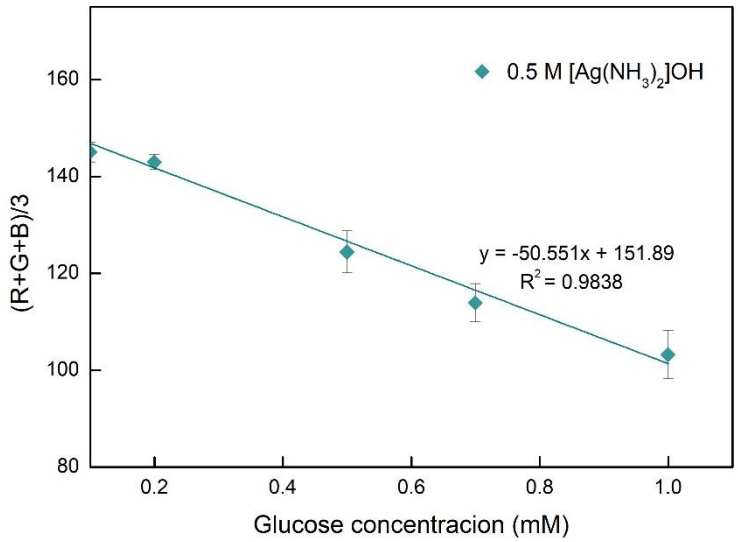

***Figure 20**- Calibration line of the RGB intensities variation with glucose under the optimized conditions on paper.*

As observed, it is possible to define a linear relation between RGB intensities in a glucose range from 0.1 to 1mM. Regarding the linearity obtained for the RGB mean intensities, it is possible to use the formation of the Au@Ag core-shell NPs in detection and measurement of glucose concentrations

The LOD of the assay was calculated and is equal to 0.121 mM. With a LOD ≈ 0.12, this strategy is indicated for a detection of glucose preferentially in hyperglycaemic patients, whose sweat glucose concentration values varies from 0.1 to 1mM.

Hence, sweat glucose diabetic values can be associated to RGB intensity values below 146.84, however the linearity obtained doesn't include glucose values in a range from 0 to 0.1 and the dispersion of results its significant for higher glucose levels.

3.3.1. SEM-EDS

SEM-EDS analysis was performed in different stages of the process to observe and analyse the formation of the bimetallic Au-Ag core-shell NPs on paper. Firstly, the effect of pre-mixing the Au and Ag precursor solutions was studied, and SEM-EDS images of the solution deposited on paper before the addition of glucose are presented in **Figure 21**.

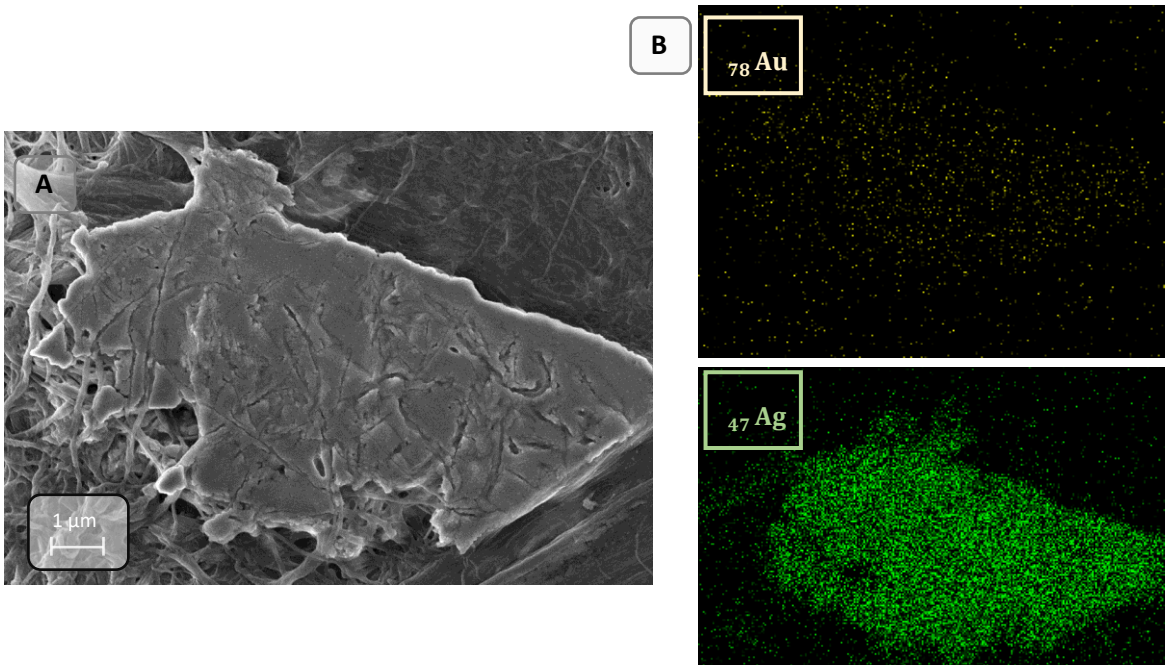

***Figure 21**- SEM image (A) and EDS element distribution map (B) of Whatman paper containing the pre-mixed solution of the Au-core and Ag-shell precursors.*

When the AuNP colloidal solution is pre-mixed with the silver precursor solution and then deposited on paper, it is possible to observe the presence of plate-shape structures along the paper fibres; EDS analysis revealed that the structures observed consist in large agglomerates of Ag covering the existent AuNPs, what goes in accordance with the visual results that suggested the non-formation of the bimetallic NPs with this method.

On the other hand, in SEM images of the solutions deposited and dried separately, is possible to observe small AuNPs adsorbed along the paper fibres. The EDS analysis revealed wide areas of presence of Au for all the sample, detecting also the presence of Ag surrounding the AuNPs spread over the sample (**Figure 22**).

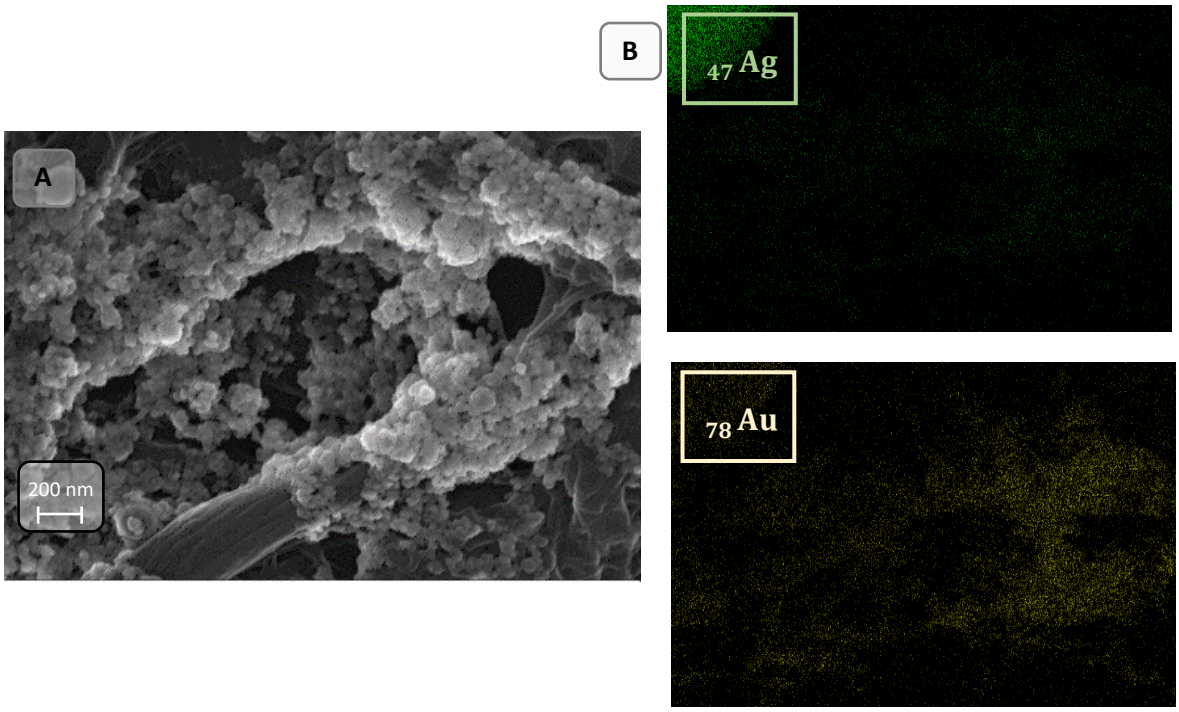

***Figure 22**- SEM image (A) and EDS element distribution map (B) of the Au-core and Ag-shell precursors deposited separately on Whatman paper.*

Following, SEM-EDS analysis was used to study the effect of adding glucose in different concentrations to the paper already containing the Au@Ag core-shell NPs precursors.

SEM images of two paper samples containing 0.2 and 1 mM of glucose (deposited 15 hours before the analysis) are presented on **Figure 23**.

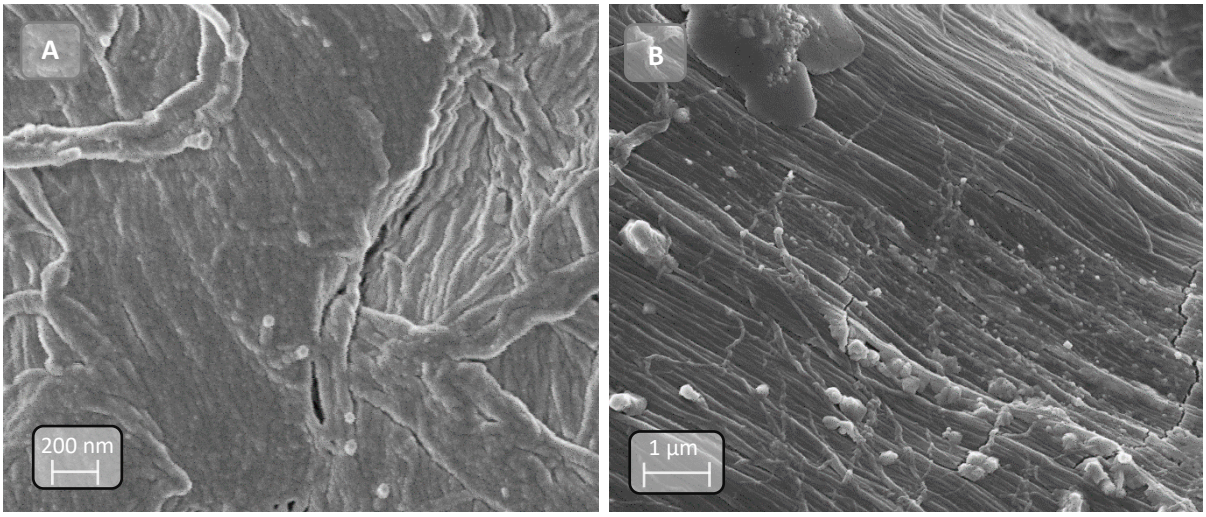

***Figure 23**- SEM images of Whatman paper containing Au@Ag core-shell bimetallic NPs obtained with (A) 0.2 mM glucose and (B) 1 mM glucose concentration.*

Analysing the SEM images in **Figure 23** is possible to identify for both glucose concentrations the presence of round-shaped structures indicating the formation of the Au@Ag core-shell bimetallic NPs. Several differences may be pointed when comparing both images, as in the sample with less glucose concentration, small white dots identified as the bimetallic NPs (**Figure 23-A**) appear in a fewer

amount and its diameter is substantially smaller. In SEM images of paper containing 1 mM of glucose (**Figure 23-B**) is possible to observe paper fibres impregnated with a large quantity of bimetallic NPs with larger diameters.

In order to identify more accurately the differences between the bimetallic NPs formed with 0.2- and 1 -mM glucose concentration, the average diameter of the bimetallic NPs (with n=8) was measured using *Image J* software and is presented on **Table 3**

***Table 3**- Average diameter of the Au@Ag core-shell bimetallic NPs obtained with 0.2 mM and 1 mM of glucose.*

Glucose concentration (mM)	Average Diameter (nm)
0.2	45.429
1	165.841

As observed in solution, also on paper the average diameter of the bimetallic NPs has increased in the presence of glucose. Comparing the NPs produced with different glucose concentrations, an increasement of approximately 100 nm can be associated to a glucose variation of ≈ 0.8 mM, which is a sufficient size variation to produce the colorimetric alterations observed on paper.

An EDS analysis were performed to identify the Ag and Au element composition and its distribution on a paper sample containing Au@Ag core-shell bimetallic NPs produced with 1 mM of glucose (**Figure 24**).

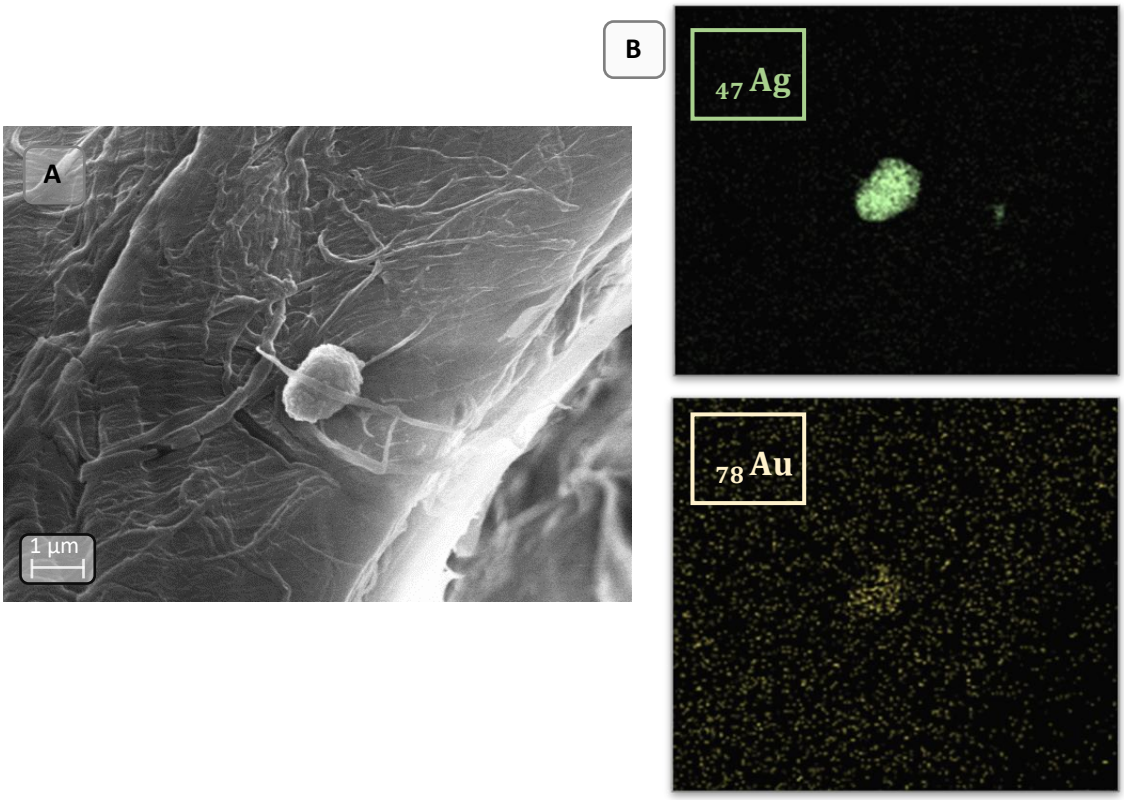

***Figure 24**- SEM image and EDS element distribution map of an Au@Ag bimetallic nanostructure produced on paper with 1 mM glucose.*

Considering EDS images in **Figure 24** is possible to identify a semi-spherical structure identified as a bimetallic NP, as the distribution map in that area reveals a very intense emission of the Ag element, with a corresponding but weaker emission of Au for the same analysed area.

However, when analysing the cumulative spectrum of the larger bimetallic NPs adsorbed on the paper fibres, the presence of Au cannot always be detected (**Figure 25**).

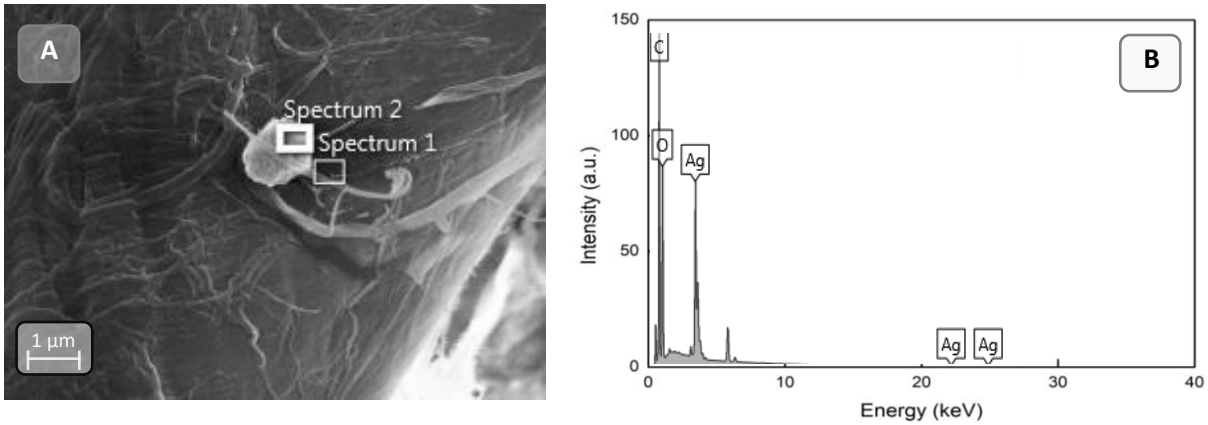

***Figure 25**- Cumulative spectrum (B) of a large nanostructure (A- Spectrum 2) obtained on paper with 1 mM of glucose (diameter ≈ 1 µm) where Au presence is not detected.*

Although, this may be due to the fact that in the presence of glucose in higher concentrations, there is a higher quantity of generated Ag^+ ions around the AuNPs, highly increasing the thickness of the silver shell. As the diameter of the AuNPs in the system is approximately 10 nm, it is possible that an Ag shell of near 1 µm of thickness inhibit the Au detection.

3.4. Prototype and estimated cost of the final device

A prototype based on the lab-on-paper technology was developed for the colorimetric detection and quantification of glucose aqueous solutions in a concentration range from 0.1 to 1 mM (**Figure 27**).

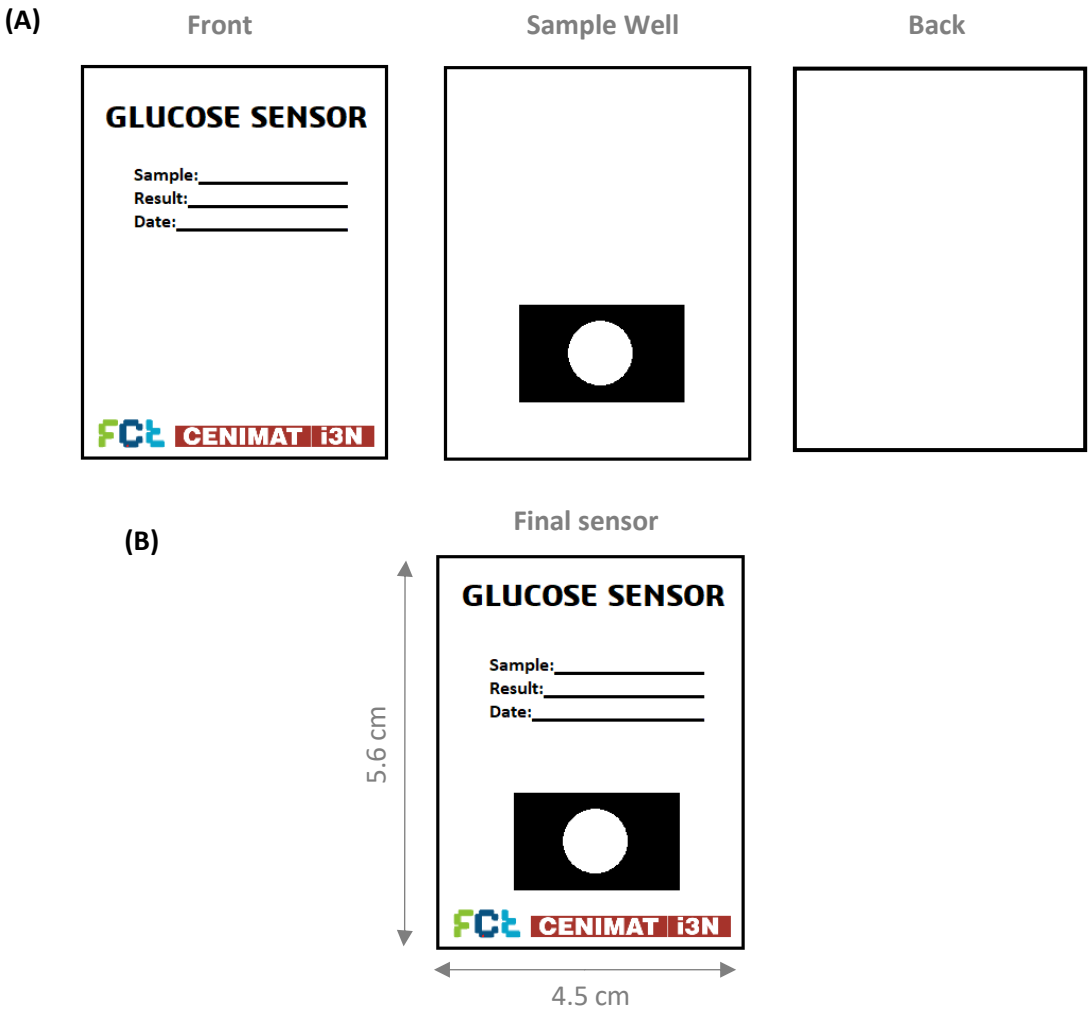

***Figure 26**- Prototype of the glucose sensor. (A) Schematic of the frontal, well and back part of the sensor (B) Frontal scheme view of the final sensor.*

The sample well must be printed and diffused on paper and then the front and back are encapsulated with wax.

In **Table 4** is presented the estimated cost of the prototyped sensor taking into account the materials and reagents used.

***Table 4**- Production cost of the prototyped sensor for glucose measurement.*

Material	Quantity	Cost	Cost/sensor
Whatman Paper nº 1	5.6 × 4.5 cm^2	5.30€/m^2	0.0132 €
Wax printing	3 × (5.6 × 4.5) cm^2	0.28€/m^2	2.11×10^{-3} €
$AgNO_3$	400 µl= 6.77 mg	4.48€/g	0.03 €
Ammonium Hydroxide	70 µl	1.08€/ml	0.0756 €
NaOH	200 µl= 6.43 mg	0.92€/g	5.91×10^{-3} €
$HAuCl_4$	50 µl =0.59mg	61.92€/g	0.0365 €
Sodium Citrate	50 µl =0.49mg	0.11€/g	5.39×10^{-5} €
Total			**0.163 €**

3.5. Storage condition's assay

In order to determine the best storage conditions for the developed sensor, the ambient conditions influence on the paper devices was studied. For that propose, the average intensities of the RGB channels of the paper substrates was monitored over the time in different environmental conditions (**Figure 26**).

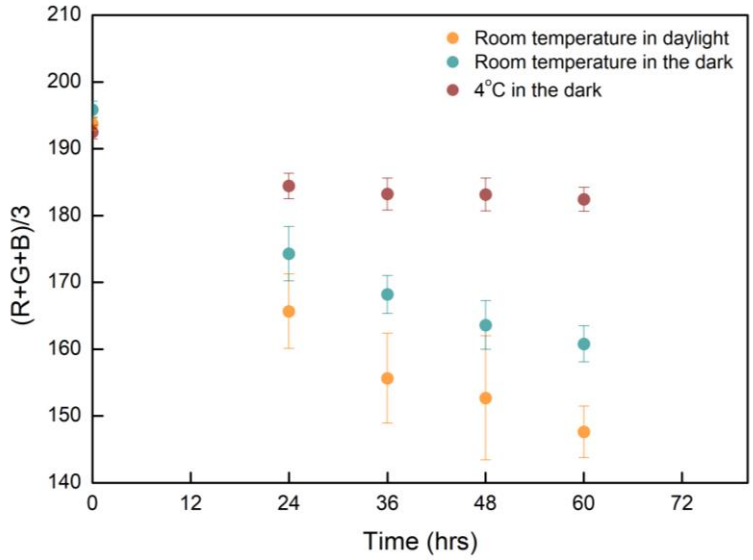

***Figure 27**- Average RGB intensities analysis of paper substrates containing the Au@Ag core-shell NPs precursors in different storage conditions.*

Analyzing the graphic is possible to observe a decrease in the RGB intensity for all the papers after the first 24 hours, however this decrease is more accentuated for the devices stored at room temperature. This behavior may be explained by the previously identified reaction of Ag with the sulfur present in the air (**5**), as the samples at room temperature were also exposed to the room air.

$$4\,Ag\,(s) + 2H_2S\,(g) + \,O_2 \Leftrightarrow \,2\,Ag_2S\,(s) + 2\,H_2O\,(l) \quad (5)$$

The accentuated decrease in the RGB channel intensities of the devices stored in daylight suggests that light facilitates the above described reaction that originates the black coloured silver sulfide compound (a lower RGB intensity means a colour closest to black).

Conclusions and future prespectives

The present work was developed with the aim of creating a paper-based platform for a highly sensitive colorimetric glucose detection, based on the formation of Au@Ag core-shell bimetallic NPs, whose Ag-shell formation and thickness is glucose dependent. The described reaction was performed in solution and it was possible to obtain a linear relation between the glucose concentrations tested (from 0.1 – to 1 – mM) and the UV-Vis absorbance values measured at 422 nm. The increase on the absorbance values indicates that the silver-shell thickness of the bimetallic NPs in solution is increasing.

To perform this sensitive glucose detection assay on paper, two different paper types were analysed in the present work: common office paper and Whatman paper nº1. Whatman paper was chosen for the development of the colorimetric assays for glucose detection, as it presented better chemical, morphological and structural features than office paper, such as an higher porosity and also the presence of less amorphous components, as proved by XRD structural analysis, where an higher crystallinity index was obtained for Whatman paper and by chemical analysis, where the presence of $CaCO_3$ on office paper was revealed.

The production of the colorimetric glucose sensing platforms was based on the Lab-on-paper technology, with wax printed test zones that are diffused along the Whatman paper, creating well-defined hydrophobic barriers that constringe the deposited liquids. An unsuccessful attempt of eliminating one deposition step was performed by mixing the bimetallic NPs precursor solutions before the deposition on paper, with SEM-EDS analysis revealing the formation of large Ag aggregates on the paper. It was concluded that AuNPs should be stabilized on paper before the addiction of the silver precursor ($Ag(NH_3)_2OH$).

After obtaining visible colorimetric variations (from light to dark brown) on paper when increasing the glucose concentration, the reagents concentration influence on the results was studied, as well as the optimal volume for deposition, that was set as 3.5 µL (paper test zones with ≈ 7 mm diameter). For the colorimetric variation analysis, the paper substrates were scanned and the RGB channel mean intensities were obtained with *Image-J software*.

The highest AuNPs colloidal solution concentration was found to be the ideal for this reaction, as it presented an enhancement of the visible signal. The Ag-shell precursor concentration was also tested, with results showing that a 0.5 M $Ag(NH_3)_2OH$ concentration is the ideal to be used for a low concentration glucose detection. For the described optimal conditions, a linear response was obtained for the RGB channel intensities in function of the glucose concentration. With an estimated LOD ≈ 0.12 mM, the proposed strategy may be developed for the measurement of glucose concentration levels in the range of hyperglycaemic patients' sweat (that are typically in a known range from 0.1 to 1 mM).

The colorimetric differences observed are related to the size variation of the bimetallic NPs adsorved on the paper surface, as the SEM-EDS analysis performed on paper revealed. The particle medium diameters increased from ≈ 40 to 115 nm, with a glucose variation from 0.2 to 1 mM. Through EDS analysis of the relative Ag and Au elements concentration in solution, is possible to conclude that the NPs size variation is due to a growth on the thickness of the Ag-shell, with an Ag/Au ratio growth from ≈ 3 to 30% with a glucose variation from 0.2 to 1 mM. A performed storage condition's assay demonstrated that the paper-sensor developed is sensitive to the temperature and to room air exposure, therefore it must be stored at 4°C and protected from the air and the light.

As the sweat glucose values measured for hypoglycaemic patients are near 0.01 mM, it would be interesting to study the application of this strategy for glucose concentrations below 0.1 mM. Additionally, and in order to apply the sensor in real sweat samples, interference tests with biological elements present in human sweat may be performed, as well as calibration optimization assays for the RGB measurements of the colorimetric changes on paper.

References

[1] A. P. F. Turner and J. C. Pickup, "Diabetes mellitus: biosensors for research and management," *Biosensors*, vol. 1, no. 1, pp. 85–115, Jan. 1985.

[2] "Diabetes." [Online]. Available: https://www.who.int/news-room/fact-sheets/detail/diabetes. [Accessed: 01-Mar-2020].

[3] D. M. Nathan, "The diabetes control and complications trial/epidemiology of diabetes interventions and complications study at 30 years: Overview," *Diabetes Care*, vol. 37, no. 1, pp. 9–16, Jan. 2014.

[4] H. Lee *et al.*, "A graphene-based electrochemical device with thermoresponsive microneedles for diabetes monitoring and therapy," *Nature Nanotechnology*, vol. 11, no. 6, pp. 566–572, Jun. 2016.

[5] A. J. Bandodkar, W. Jia, C. Yardimci, X. Wang, J. Ramirez, and J. Wang, "Tattoo-based noninvasive glucose monitoring: A proof-of-concept study," *Analytical Chemistry*, vol. 87, no. 1, pp. 394–398, Jan. 2015.

[6] B. A. Katchman, M. Zhu, J. Blain Christen, and K. S. Anderson, "Eccrine Sweat as a Biofluid for Profiling Immune Biomarkers," *Proteomics - Clinical Applications*, vol. 12, no. 6, p. 1800010, Nov. 2018.

[7] I. Journal and I. Factor, "BioMed Research International (J BIOMED BIOTECHNOL)," *http://dx.doi.org/10.1155/2015/431047*, vol. 2015, pp. 2–4, 2015.

[8] J. Moyer, D. Wilson, I. Finkelshtein, B. Wong, and R. Potts, "Correlation between sweat glucose and blood glucose in subjects with diabetes," *Diabetes Technology and Therapeutics*, vol. 14, no. 5, pp. 398–402, May 2012.

[9] D. Bruen, C. Delaney, L. Florea, and D. Diamond, "Glucose Sensing for Diabetes Monitoring: Recent Developments," *Sensors*, vol. 17, no. 8, p. 1866, Aug. 2017.

[10] N. Brasier and J. Eckstein, "Sweat as a Source of Next-Generation Digital Biomarkers," pp. 155-165, Dec. 2019.

[11] A. Martín *et al.*, "Epidermal Microfluidic Electrochemical Detection System: Enhanced Sweat Sampling and Metabolite Detection," *ACS Sensors*, vol. 2, no. 12, pp. 1860–1868, Dec. 2017.

[12] A. Mena-Bravo and M. D. Luque de Castro, "Sweat: A sample with limited present applications and promising future in metabolomics," *Journal of Pharmaceutical and Biomedical Analysis*, vol. 90. Elsevier, pp. 139–147, 05-Mar-2014.

[13] I. Turner, Anthony; Wilson, George; Kaube, "*Biosensors: Fundamentals and Applications*." Oxford, UK: Oxford University Press, pp. 180-210, 1987.

[14] S. P. Mohanty and E. Koucianos, "Biosensors: A tutorial review," *IEEE Potentials*, vol. 25, no. 2. pp. 35–40, 2006.

[15] M. Holzinger, A. le Goff, and S. Cosnier, "Nanomaterials for biosensing applications: A review," *Frontiers in Chemistry*, vol. 2, no. AUG. Frontiers Media S. A, 2014.

[16] H. R. Zare and Z. Shekari, "Types of monitoring biosensor signals," in *Electrochemical Biosensors*, Elsevier, pp. 135–166, 2019.

[17] C. Dincer *et al.*, "Disposable Sensors in Diagnostics, Food, and Environmental Monitoring," *Advanced Materials*, vol. 31, no. 30. Wiley-VCH Verlag, 26-Jul-2019.

[18] "Biosensor - an overview | ScienceDirect Topics." Available: *https://www.sciencedirect.com/topics/chemistry/biosensor.* [Accessed: 01-Mar-2019].

[19] Q.-L. Liu *et al.*, "Electrochemical Enzyme-Linked Immunosorbent Assay (ELISA) for α-Fetoprotein Based on Glucose Detection with Multienzyme-Nanoparticle Amplification," *Molecules*, vol. 18, no. 10, pp. 12675–12686, Oct. 2013.

[20] A. Nilghaz, L. Guan, W. Tan, and W. Shen, "Advances of Paper-Based Microfluidics for Diagnostics—The Original Motivation and Current Status," *ACS Sensors*, vol. 1, no. 12, pp. 1382–1393, Dec. 2016.

[21] J. Nie *et al.*, "Low-Cost Fabrication of Paper-Based Microfluidic Devices by One-Step Plotting," *Analytical Chemistry*, vol. 84, no. 15, pp. 6331–6335, Aug. 2012.

[22] J. Hu *et al.*, "Advances in paper-based point-of-care diagnostics," *Biosensors and Bioelectronics*, vol. 54. Elsevier Ltd, pp. 585–597, 15-Apr-2014.

[23] K. Mahato, A. Srivastava, and P. Chandra, "Paper based diagnostics for personalized health care: Emerging technologies and commercial aspects," *Biosensors and Bioelectronics*, vol. 96. Elsevier Ltd, pp. 246–259, 15-Oct-2017.

[24] A. K. Yetisen, M. S. Akram, and C. R. Lowe, "Paper-based microfluidic point-of-care diagnostic devices," *Lab on a Chip*, vol. 13, no. 12. Royal Society of Chemistry, pp. 2210–2251, 21-Jun-2013.

[25] B. Gao, X. Li, Y. Yang, J. Chu, and B. He, "Emerging paper microfluidic devices," *Analyst*, vol. 144, no. 22. Royal Society of Chemistry, pp. 6497–6511, 21-Nov-2019.

[26] K. Stana-Kleinschek, S. Strnad, and V. Ribitsch, "Surface characterization and adsorption abilities of cellulose fibers," *Polymer Engineering and Science*, vol. 39, no. 8, pp. 1412–1424, Aug. 1999.

[27] S. Kumar, P. Bhushan, and S. Bhattacharya, "Fluid Transport Mechanisms in Paper-Based Microfluidic Devices," 2019, pp. 7–28.

[28] A. W. Martinez, S. T. Phillips, M. J. Butte, and G. M. Whitesides, "Patterned paper as a platform for inexpensive, low-volume, portable bioassays," *Angewandte Chemie - International Edition*, vol. 46, no. 8, pp. 1318–1320, 2007.

[29] K. Abe, K. Suzuki, and D. Citterio, "Inkjet-printed microfluidic multianalyte chemical sensing paper," *Analytical Chemistry*, vol. 80, no. 18, pp. 6928–6934, Sep. 2008.

[30] C. M. Cheng *et al.*, "Millimeter-scale contact printing of aqueous solutions using a stamp made out of paper and tape," *Lab on a Chip*, vol. 10, no. 23, pp. 3201–3205, Dec. 2010.

[31] E. M. Fenton, M. R. Mascarenas, G. P. López, and S. S. Sibbett, "Multiplex lateral-flow test strips fabricated by two-dimensional shaping," *ACS Applied Materials and Interfaces*, vol. 1, no. 1, pp. 124–129, Jan. 2009.

[32] Z. Nie *et al.*, "Electrochemical sensing in paper-based microfluidic devices," *Lab on a Chip*, vol. 10, no. 4, pp. 477–483, 2010.

[33] R. Lu, W. Shi, L. Jiang, J. Qin, and B. Lin, "Rapid prototyping of paper-based microfluidics with wax for low-cost, portable bioassay," *Electrophoresis*, vol. 30, no. 9, pp. 1497–1500, May 2009.

[34] G. Grau, "Low-cost fabrication of paper-based systems: Microfluidics, sensors, electronics and deployment," in *Midwest Symposium on Circuits and Systems*, 2017, vol. 2017-Augus, pp. 84–87.

[35] M. N. Costa *et al.*, "A low cost, safe, disposable, rapid and self-sustainable paper-based platform for diagnostic testing: Lab-on-paper," *Nanotechnology*, vol. 25, no. 9, Mar. 2014.

[36] T. S. Park, W. Li, K. E. McCracken, and J. Y. Yoon, "Smartphone quantifies Salmonella from paper microfluidics," *Lab on a Chip*, vol. 13, no. 24, pp. 4832–4840, Dec. 2013.

[37] Q. Kong, Y. Wang, L. Zhang, S. Ge, and J. Yu, "A novel microfluidic paper-based colorimetric sensor based on molecularly imprinted polymer membranes for highly selective and sensitive detection of bisphenol A," *Sensors and Actuators, B: Chemical*, vol. 243, pp. 130–136, May 2017.

[38] A. Yakoh, P. Rattanarat, W. Siangproh, and O. Chailapakul, "Simple and selective paper-based colorimetric sensor for determination of chloride ion in environmental samples using label-free silver nanoprisms," *Talanta*, vol. 178, pp. 134–140, Feb. 2018.

[39] A. Carolina C. Marques, "*Desenvolvimento de um sensor colorimétrico em papel para a deteção de bactérias eletroquimicamente ativas*," FCT-UNL, 2014.

[40] S. Unser, I. Campbell, D. Jana, and L. Sagle, "Direct glucose sensing in the physiological range through plasmonic nanoparticle formation," *Analyst*, vol. 140, no. 2, pp. 590–599, Jan. 2015.

[41] H. Zhu, L. Li, W. Zhou, Z. Shao, and X. Chen, "Advances in non-enzymatic glucose sensors based on metal oxides," *Journal of Materials Chemistry B*, vol. 4, no. 46. Royal Society of Chemistry, pp. 7333–7349, 23-Nov-2016.

[42] M. Li, L. Shi, T. Xie, C. Jing, G. Xiu, and Y.-T. Long, "An Ultrasensitive Plasmonic Nanosensor for Aldehydes," *ACS Sensors*, vol. 2, no. 2, pp. 263–267, Feb. 2017.

[43] L. R. Soares, "*Nanopartículas de ouro anisométricas como nanossondas para a identificação do polimorfismo de DNA associado à Intolerância à Lactose",* FCT-UNL, 2016.

[44] Q. Zhu, X. Zhang, Y. Wang, A. Zhu, R. Gao, and X. Zhao, "Controlling the Growth Locations of Ag Nanoparticles at Nanoscale by Shifting LSPR Hotspots," *Nanomaterials* 2019.

[45] S. K. Ghosh and T. Pal, "Interparticle coupling effect on the surface plasmon resonance of gold nanoparticles: From theory to applications," *Chemical Reviews*, vol. 107, no. 11. pp. 4797–4862, Nov-2007.

[46] Y. Li, H. J. Schluesener, S. Xu, and W. G. Org, "Gold nanoparticle-based biosensors," *Gold Bull,* vol. 43, pp. 29–41, 2010.

[47] Alizadeh, S., Nazari, Z., "A Review on Gold Nanoparticles Aggregation and Its Applications", *Journal of Chemical Reviews*, pp. 228-242, (2020).

[48] N. D. Samsuri, W. M. Mukhtar, A. R. A. Rashid, K. A. Dasuki, and A. A. R. Hj. A. Yussuf, "Synthesis methods of gold nanoparticles for Localized Surface Plasmon Resonance (LSPR) sensor applications," *EPJ Web of Conferences*, vol. 162, p. 1002, 2017.

[49] W. S. Hwang, P. L. Truong, and S. J. Sim, "Size-dependent plasmonic responses of single gold nanoparticles for analysis of biorecognition," *Analytical Biochemistry*, vol. 421, no. 1, pp. 213–218, Feb. 2012.

[50] W. Lu *et al.*, "Multifunctional oval-shaped gold-nanoparticle-based selective detection of breast cancer cells using simple colorimetric and highly sensitive two-photon scattering assay," *ACS Nano*, vol. 4, no. 3, pp. 1739–1749, Mar. 2010.

[51] G. Maduraiveeran, R. Rasik, M. Sasidharan, and W. Jin, "Bimetallic gold-nickel nanoparticles as a sensitive amperometric sensing platform for acetaminophen in human serum," *Journal of Electroanalytical Chemistry*, vol. 808, pp. 259–265, Jan. 2018.

[52] Y. Gao, Y. Wu, and J. Di, "Colorimetric detection of glucose based on gold nanoparticles coupled with silver nanoparticles," *Spectrochimica Acta - Part A: Molecular and Biomolecular Spectroscopy*, vol. 173, pp. 207–212, Feb. 2017.

[53] F. Kang, X. Hou, and K. Xu, "Highly sensitive colorimetric detection of glucose in a serum based on DNA-embeded Au@Ag core-shell nanoparticles.," *Nanotechnology*, vol. 26, no. 40, p. 405707, Oct. 2015.

[54] Y. Lu *et al.*, "Fabrication and characterization of a highly-sensitive surface-enhanced Raman scattering nanosensor for detecting glucose in urine," *Nanomaterials*, vol. 8, no. 8, Aug. 2018.

[55] M. Li, L. Shi, T. Xie, C. Jing, G. Xiu, and Y. T. Long, "An Ultrasensitive Plasmonic Nanosensor for Aldehydes," *ACS Sensors*, vol. 2, no. 2, pp. 263–267, Feb. 2017.

[56] T. Li *et al.*, "Sensitive detection of glucose based on gold nanoparticles assisted silver mirror reaction," *Analyst*, vol. 136, no. 14, pp. 2893–2896, Jul. 2011.

[57] "A low cost, safe, disposable, rapid and self-sustainable paper-based platform for diagnostic testing: Lab-on-paper.", *Nanotechnology,* Vol. 25, No. 9, pp. 094006, Feb. 2014.

[58] V. Hospodarova, E. Singovszka, and N. Stevulova, "Characterization of Cellulosic Fibers by FTIR Spectroscopy for Their Further Implementation to Building Materials," *American Journal of Analytical Chemistry*, vol. 09, no. 06, pp. 303–310, 2018.

[59] L. Segal, J. J. Creely, A. E. Martin, and C. M. Conrad, "An Empirical Method for Estimating the Degree of Crystallinity of Native Cellulose Using the X-Ray Diffractometer," *Textile Research Journal*, vol. 29, no. 10, pp. 786–794, Oct. 1959.

[60] S. Park, J. O. Baker, M. E. Himmel, P. A. Parilla, and D. K. Johnson, "Cellulose crystallinity index: Measurement techniques and their impact on interpreting cellulase performance," *Biotechnology for Biofuels*, vol. 3, 2010.

[61] X. Huang and M. A. El-Sayed, “Gold nanoparticles: Optical properties and implementations in cancer diagnosis and photothermal therapy,” *Journal of Advanced Research*, vol. 1, no. 1. Elsevier, pp. 13–28, 01-Jan-2010.

[62] Y. Dong, H. Zhu, Y. Shen, W. Zhang, and L. Zhang, “Antibacterial activity of silver nanoparticles of different particle size against Vibrio Natriegens,” *PLoS ONE*, vol. 14, no. 9, p. e0222322, 2019.

[63] JCE staff, “Silver to Black - and Back,” *Journal of Chemical Education*, vol. 77, no. 3, p. 328A, Mar. 2000.

[64] “RGB (Red Green Blue) Definition.”, *Available: https://techterms.com/definition/rgb,* [Accessed: 27-Mar-2019].

[65] S. Szunerits, J. Spadavecchia, and R. Boukherroub, “Surface plasmon resonance: Signal amplification using colloidal gold nanoparticles for enhanced sensitivity,” *Reviews in Analytical Chemistry*, vol. 33, no. 3, pp. 153–164, Oct. 2014.

Appendicces

A. Absorbance spectra of the bimetallic NPs solution

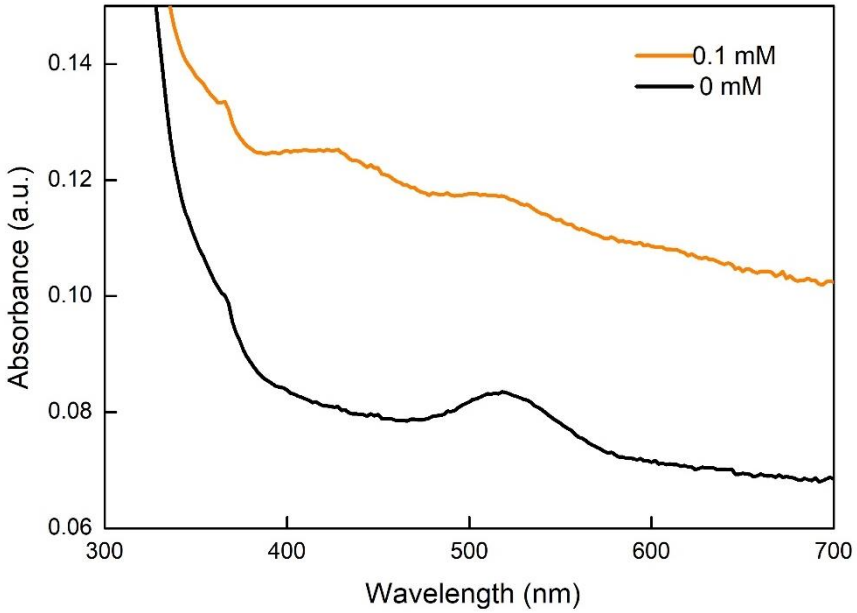

***Figure 28**-UV-Vis Absorbance spectra of solutions containing Au@Ag core-shell NPs obtained for 0.1 and 1 mM glucose concentrations.*

B. EDS cumulative spectra and element quantification table of a bimetallic NP in solution with 0.2 and 1 mM glucose.

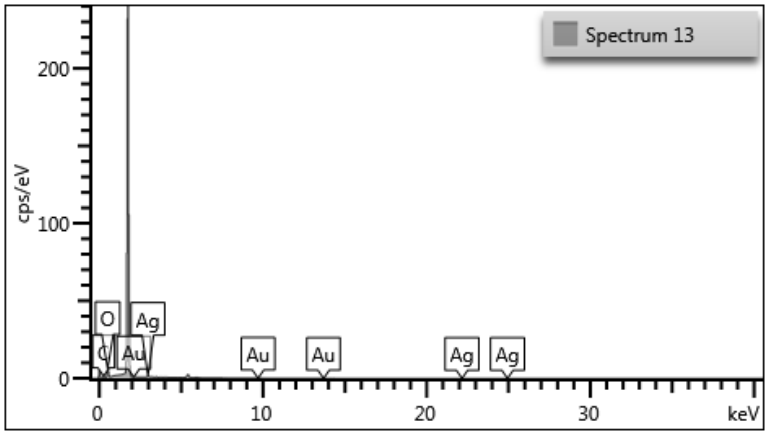

***Figure 29**- EDS cumulative spectra of a bimetallic NP in solution with 0.2 mM glucose.*

***Table 5**- EDS element quantification table of a bimetallic NP in solution with 0.2 mM glucose*

Element	k Ratio	Wt%	Wt% Sigma
C	0.00000	0.00	0.00
O	0.00119	61.76	2.71
Ag	0.00133	29.94	2.32
Au	0.00035	8.30	2.54

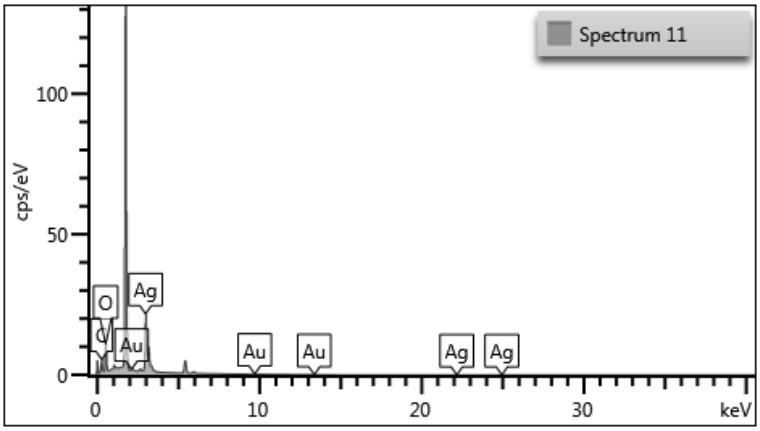

***Figure 30**- EDS cumulative spectra of a bimetallic NP in solution with 1 mM glucose.*

***Table 6**- EDS element quantification table of a bimetallic NP in solution with 1 mM glucose*

Element	Wt%	Atomic %	Element
C	0.00	0.00	C
O	28.60	73.26	O
Ag	69.19	26.28	Ag
Au	2.21	0.46	Au

C. Variation of the AuNPs colloidal solution concentration

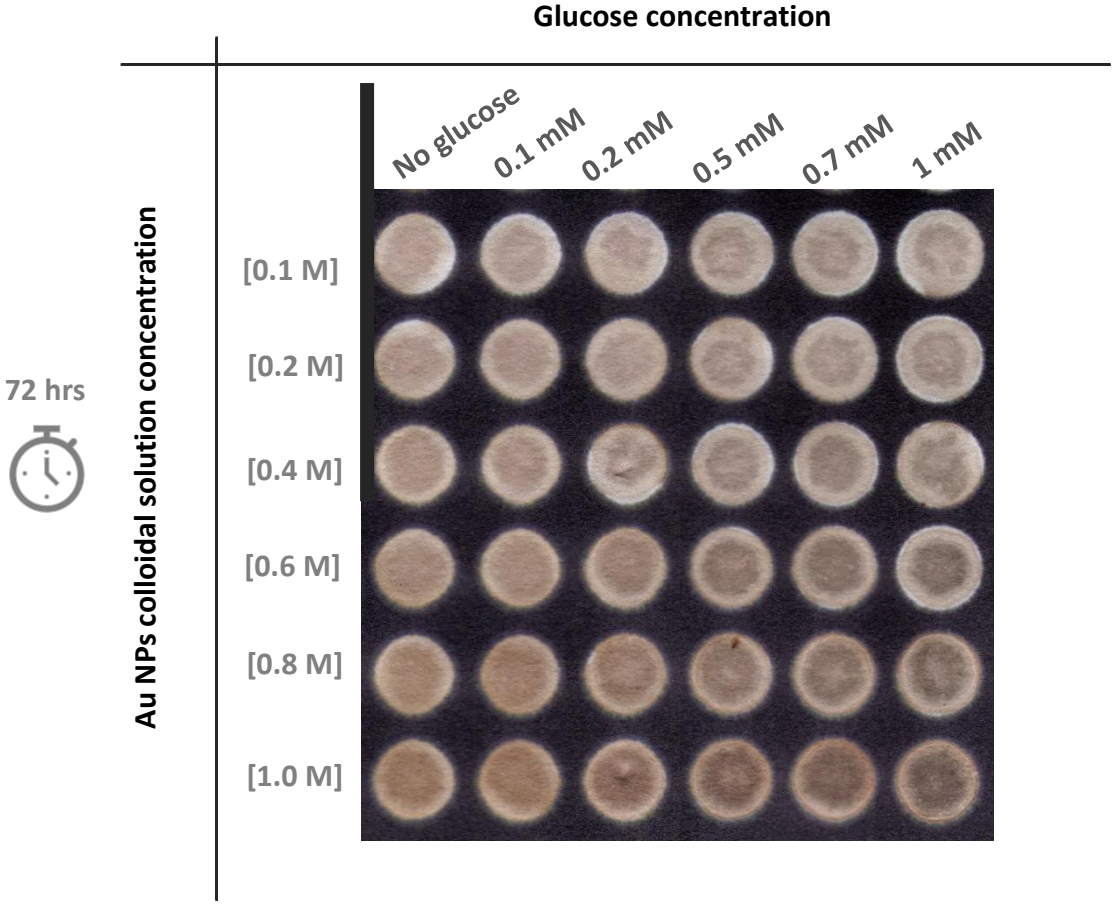

***Figure 31**- Influence of the AuNPs colloidal solution concentration on the Au@Ag core-shell bimetallic NPs synthesis on paper with glucose.*

D. RGB analysis of the paper microplates containing different $Ag(NH_3)_2OH$ concentrations and calibration lines

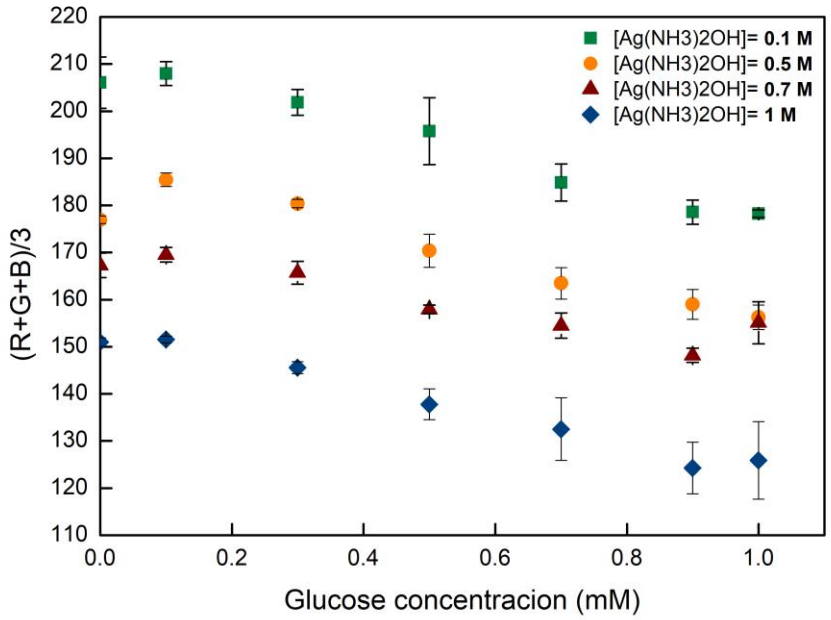

***Figure 32**- RGB analysis of the paper microplates containing different $Ag(NH_3)_2OH$ concentrations.*

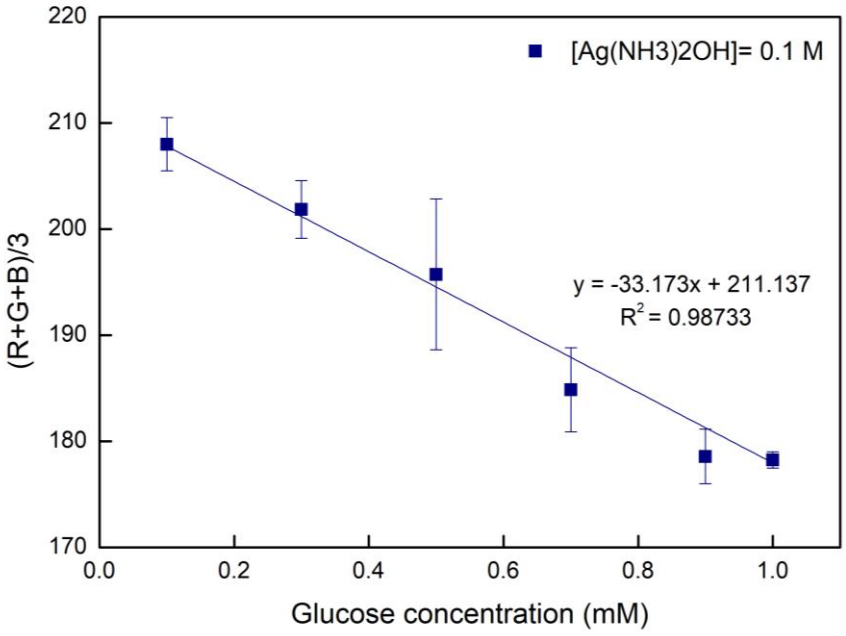

***Figure 33**- Calibration line for 0.1 M $Ag(NH_3)_2OH$.*

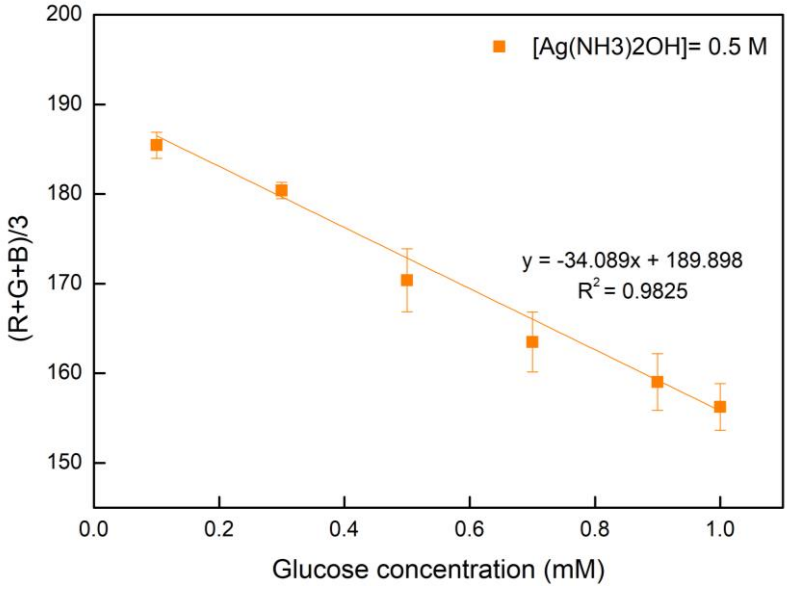

***Figure 34**- Calibration line for 0.5 M Ag(NH3)2OH*

.

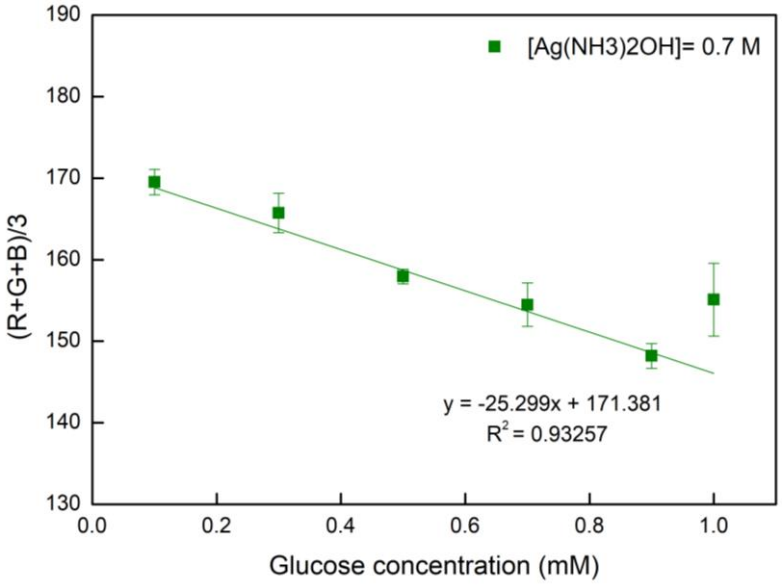

***Figure 35**- Calibration line for 0.7 M Ag(NH3)2OH*

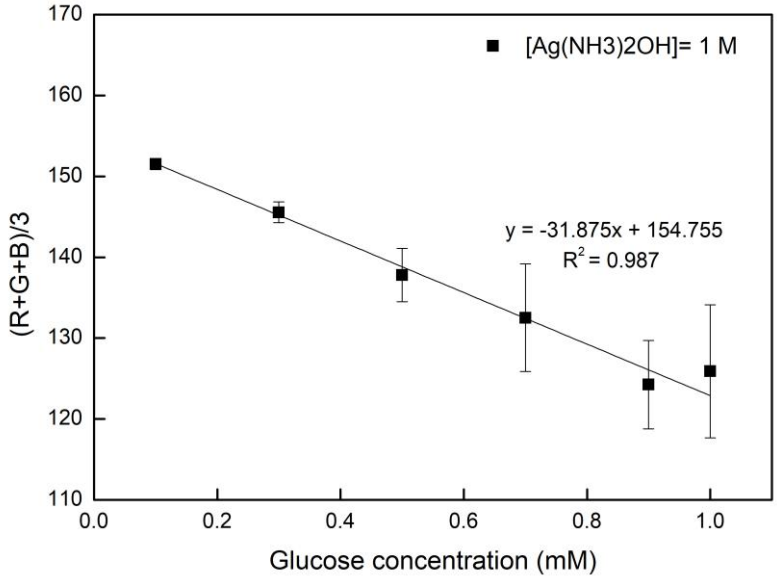

***Figure 36**- Calibration line for 1 M Ag(NH3)2OH*